

# RESEARCH ON THE FATIGUE BEHAVIOR OF THE P1030 CEMENTED CARBIDE GRADE

**Bas Letschert**

*March 2011*

**FINAL VERSION**

**Final thesis**

Mechanical Engineering - Integrated Product Development

Faculty 'Natuur & Techniek'

University of Applied Sciences Utrecht (HU)

**Author** S.P. Letschert

**Student number** 1536592

**Company** Philips Consumer Lifestyle B.V.

**Department** Process Engineering K&H

**Address** Oliemolenstraat 5  
9203 ZN Drachten

**Supervisors** HU: ir. M. Pallada  
ing. R. Müller  
Philips: ir. J.B.H. Silvius





## PREFACE

Normally at the Utrecht University of Applied Sciences (HU) it is common to do projects on how an apparatus is designed and engineered and which choices are made in these phases. Because I had the change to do these kinds of projects during the regular educational program I tried to approach my final internship differently.

The major difference between this project and the previous projects in the regular program is that this project goes much more into deep covering only one specific subject instead of using available, more common information about different subjects and combining it into an engineering solution. I have to say that this, for me new approach was challenging but I really enjoyed it.

### Acknowledgements

First of all I would like to thank Martin van Veen for giving me the opportunity do this final internship at Philips Consumer Lifestyle in Drachten.

I'm very, very thankful for the daily support of Johannes Silvius as my internship coordinator. Especially the freedom to define my own subject and boundary conditions was very pleasant. His faith in a good result, despite the given freedom, motivated me to do my utmost best. The great atmosphere in our day to day contact in the department I appreciated very much!

Special thanks go out to Ronald v/d Linden for explaining me the first and probably most important things about cemented carbides, helping me out with the test setup and his support during the tests. Also Albert v/d Marel, Alex Punter and Marijke de Vries I would like to thank because of their help with respectively the ordering of the specimens, the help with the SEM and the Alicona measurements.

I would also like to thank the colleagues present in office AU B12. I had a great time with you all while working on my thesis. We had a lot of fun and I enjoyed our very interesting discussions.

And last but not least I would very much like to thank Marc Pallada and his colleague Rob Müller for their support during this final internship. I was always good informed by the demands on the final report and the deadlines. The feedback they had was always constructive(!) and thus helping me very much in writing this report.

Everybody that I forgot to incorporate into this section but belonging here: thank you very much!



## SUMMARY

The exceptional combination of strength and wear resistance makes cemented carbides a suitable material for usage in cold forming processes. But due to its limited ability to undergo tensile stresses failure of cold forming tools happens regularly. The reason for this failure is not always clear because the brittle behavior of this material does not disclose the reason of failure. For this reason an investigation on the fatigue behavior of cemented carbides is performed.

In the cold forming process of making a shaving cap, at the step where the running groove is flattened, the most stresses occur. The tooling in this process is therefore made of a special designed cemented tungsten carbide grade with internal code P1030. Due to the fact that this is the highest stressed process step the investigation is aimed at this cemented carbide grade.

This investigation starts with a literature study and is followed by a test phase in which some hypothesis are tested.

The literature study starts with common information about cemented carbides and its applications. This is then followed by a general research on (brittle) fracture and Linear Elastic Fracture Mechanics (LEFM). The next step is a literature study on the fatigue behavior of cemented carbides and the factors that influence this behavior.

In the test phase an attempt to generate a Wöhler-like curve is performed. Subsequently two different surface finishing techniques are compared. Finally the lifetime of a specimen subjected to cyclic loads at room temperature is compared to that of a specimen tested at 250°C.

Despite a mirror-like surface of the grinded specimens a large spread in test results is found, making it impossible to use the created Wöhler-like curve as a design parameter. But this curve indicates that this cemented carbide grade does show signs of fatigue behavior.

The results from the increased temperature tests suggest that a temperature of 250°C is beneficial to the fatigue sensitivity but also a large spread is found making it necessary to validate this with extra tests.

Furthermore it is shown that the flexural and fatigue strength of the specimens is negatively affected by the EDM process.



## TABLE OF CONTENTS

Preface	ii
Summary	iv
Table of figures	1
Nomenclature & Symbols	3
1. Introduction	5
1.1 Objective	5
1.2 Approach	6
1.3 Outline	7
2. Cemented carbides	9
2.1 History	9
2.2 What are cemented carbides?	9
2.3 How is it made?	11
2.4 Cemented carbides in shaving cap production	12
2.5 Flattening of the running groove	12
3. Fracture	15
3.1 Introduction	15
3.2 Ductile versus brittle	15
3.3 Brittle fracture	17
3.4 Linear Elastic Fracture Mechanics (LEFM)	17
3.5 Transverse rupture strength	21
4. Fatigue	25
4.1 Introduction	25
4.2 Fatigue in general	26
4.3 Fatigue failure in steps	27
4.4 Crack propagation rate (stage II crack growth)	29

4.5	Fatigue in WC-Co cemented carbides	33
5.	Test setup	39
5.1	Hypothesis and goal	39
5.2	Principle	43
5.3	Specimen	43
5.4	Equipment	48
5.5	Process	50
5.6	Results	53
6.	Conclusion	59
7.	Recommendations & future work	61
	Bibliography	63
	Appendix	i
1.	Mechanical properties	iii
2.	Wear	iv
2.1	Adhesive wear	iv
2.2	Abrasive wear	v
2.3	Corrosive wear	v
2.4	Surface fatigue	vi
3.	Specimens	vii
4.	Sample pictures	viii
5.	specimen data / Test results	xi
6.	Cemented carbide grades	xii
7.	Supplier codes	xiii
8.	P1030 standard	xv
9.	Ceratizit test report	xviii
10.	Position Aid	xix

## TABLE OF FIGURES

Figure 1-1 Evolution of Philips the shaver	5
Figure 1-2 Thesis outline explanation	8
Figure 2-1 WC-Co microstructure examined by optical (left) and scanning electron (right) microscope [2]	9
Figure 2-2 Application range of straight grade cemented carbide [3]	10
Figure 2-3 Cemented carbide production process [3]	11
Figure 2-4 Flattening the running groove	12
Figure 3-1 Fracture profiles [6]	15
Figure 3-2 Ductile to brittle transition	16
Figure 3-3 Fracture types [7]	17
Figure 3-4 (a) Geometry of surface and internal cracks. (b) Schematic stress profile along line X-X' in (a), demonstrating stress amplification at crack tip [6]	17
Figure 3-5 Beam with edge crack subjected to bending [7]	18
Figure 3-6 Fracture modes I, II and III (where I, II and III are referring to the Roman numbering system) [6]	19
Figure 3-7 Plane stress and plane strain	20
Figure 3-8 Grinded surface given super-finish [4]	21
Figure 3-9 Three point bending/flexural test [6]	22
Figure 4-1 Stress-time modes [6]	26
Figure 4-2 S-N curves of two types of fatigue behavior [6] (a) Ferrous (b) Non-ferrous	27
Figure 4-3 Beachmarks (left) and striations (right) [6]	28
Figure 4-4 Crack length vs number of cycles at two different stress levels [6]	29
Figure 4-5 Crack growth per cycle as a function of $\Delta K$ [7]	30
Figure 4-6 Simplified Paris curve [7]	32
Figure 4-7 Fatigue fracture origins: abnormal large carbide (a), subsurface pore (b) [8] and microcrack (c) [18]	33
Figure 4-8 Effect of binder mean free path on $K_{th}$ and $K_{Ic}$ (a) and on fatigue sensitivity (b) [15]	34
Figure 4-9 WC-Co frequency dependence in corrosive environment [20]	35

Figure 4-10 Temperature dependence of the cyclic loads of a cemented carbide grade [19]	36
Figure 4-11 Notched flexural fatigue of a cemented carbide grade comparable to P1030 [22]	36
Figure 4-12 Comparison of EDM'ed, EDM + annealed and polished specimens [12]	37
Figure 4-13 Cobalt distribution in WC-Co cemented carbide upon active impregnation of 8s and subsequent holding: (a) 10s, (b) 15s, (c) 20 s. Value of cobalt content (in wt%) is equal to an isoline multiplied by 6 [25].	38
Figure 5-1 Expected test results	40
Figure 5-2 Outline of test setup	42
Figure 5-3 Three point flexural test	43
Figure 5-4 Sample dimensions	44
Figure 5-5 Overview of the tensile side of the specimens: EDM, sintered and grinded (from top to bottom)	46
Figure 5-6 Overview of fatigue test equipment	48
Figure 5-7 Support used for fatigue tests (3D model)	49
Figure 5-8 Desired waveform with non-zero trough	52
Figure 5-9 Three point flexure test analysis (Force (N) x 1,5 = Stress (MPa)) [29]	53
Figure 5-10 Wöhler plot	54
Figure 5-11 Pitting on the edges of the grinded specimens (identical magnification)	55
Figure 5-12 Increased temperature test	56
Figure 5-13 EDM versus Grinding	57
Figure 5-14 Fracture analysis	58
Figure 2-1 Example of adhesive wear [4]	iv
Figure 2-2 Punch edge showing abrasive wear [4]	v
Figure 2-3 Corrosive wear on chrome steel bushing [4]	v
Figure 2-4 Surface fatigue due to rolling contact	vi
Figure 4-1 Confocal microscope pictures of specimens with different production techniques	viii
Figure 4-2 SEM pictures of sintered and grinded specimens	ix
Figure 4-3 SEM pictures of EDM'ed specimens	x

## NOMENCLATURE & SYMBOLS

$\sigma_{fs}$	Flexural strength
$\sigma_p$	Compressive strength
$\sigma_{trs}$	Transverse rupture strength
$\sigma_{max}$	Maximum stress (tensile)
$\sigma_{min}$	Minimum stress (tensile or compressive)
$\Delta\sigma$	Stress range ( $\sigma_{max}-\sigma_{min}$ )
$\sigma_0$	Nominal stress
$\sigma_c$	Critical stress
$\sigma_f$	Fatigue limit
$S$	Stress level
$N$	Number of cycles
$N_f$	Number of cycles until failure / fatigue life
$N_i$	Number of cycles for crack initiation
$N_p$	Number of cycles for crack propagation
$E$	Young's modulus / modulus of elasticity
$HV30$	Vicker hardness (with 30 kgf load)
$WK$	Palmqvist toughness
$\gamma_s$	Specific surface energy
$V_{Co}$	Binder content
$d_{WC}$	Mean carbide grain size
$\lambda_{Co}$	Binder mean free path
$C$	Material constant depending on environment, frequency, stress ratio
$m$	Material constant depending on environment, frequency, stress ratio
$a$	Length of surface crack / half length of internal crack
$a_0$	Initial crack size
$a_c$	Critical crack size
$da/dN$	Crack growth rate
$\rho_t$	Crack's radius of curvature

$Y$	Shape function for natural flaws
$K_t$	Stress concentration factor
$K_{max}$	Maximum stress intensity factor
$K_{min}$	Minimum stress intensity factor
$\Delta K$	Stress intensity factor range ( $K_{max} - K_{min}$ )
$K_c$	Critical stress intensity factor / fracture toughness
$K_{Ic}$	Plain strain fracture toughness
$K_{th}$	Threshold stress intensity factor
$K_{th}/K_{Ic}$	Fatigue sensitivity
$R$	Load ratio
$M$	Maximum bending moment
$c$	Distance from center of the specimen to the outer fiber
$I$	Moment of inertia
$F$	Applied force
$L$	Length of specimen
$b$	Width of specimen
$d$	Height of specimen
LEFM	Linear Elastic Fracture Mechanics
FCG	Fatigue Crack Growth
EDM	Electrical Discharge Machining

## 1. INTRODUCTION

Since its founding in 1891, Philips evolved from a light bulb manufacturer to one of the largest industrial companies of the world with a multinational workforce of 118.000 employees (Oct. 2010). Its mission is to “Improve the quality of people’s lives through timely introduction of meaningful innovations’.

The company exists of three divisions; Healthcare, Lighting and Consumer Lifestyle. Each division focuses on a part of people’s lives and tries to fulfill their needs and aspirations.

One of the most famous Philips products is the electrical shaver. An appliance that tries to make personal care at home easier, faster and more comfortable. Since 1939, Philips produces shavers with rotating cutters instead of reciprocating cutters that had been used in predecessors. More than 400 million shavers have been sold even since. The rotating shaver went through a lot of (r)evolutions since its first design as can be seen below.



Figure 1-1 Evolution of Philips the shaver

The Philips shavers are designed, engineered and produced at the Philips site in Drachten, one of the largest sites of Philips in the world.

### 1.1 OBJECTIVE

The cap and cutter of a shaver are produced in a cold forming process followed by multiple finishing processes. The wish is to reduce the amount of required finishing steps by improving and extending the cold forming process. This wish exists by the fact that finishing steps are relatively expensive compared to the cold forming process.

The tooling used in cold forming processes is made of cemented carbides. This material is famous for its high strength, hardness and wear resistance. But it also has a major weakness; due to its brittle nature it is not capable of undergoing large tensile stresses. The required shape of the tooling induces unavoidable tensile stresses and is limiting tool life.

In process development these days, the assumption is made that if tensile stresses in tooling are equal to, or even lower than used in current cold forming process, the tooling will survive and tool life is good enough to be

economically feasible. Due to the increasing demands on the cold forming process this way of working is no longer possible. Thus an investigation on fatigue failure of tooling is needed.

### **Goal**

For many materials fatigue failure can be predicted by so called 'Wöhler' or ' $S - N$ ' curves. These curves describe the expected life of materials under cyclic loads. The goal of this thesis is to see if it is possible, and if possible, to generate such a curve for the tooling material (internal code: P1030) used in current processes. This curve can then be used by engineers to predict the effect of tensile stresses on the tool life in new process and cap designs.

Summarizing: "This research is performed to get a better understanding of the factors that can influence the fatigue behavior of cemented carbides subjected to tensile stress. Also generating a criterion in the form of a Wöhler curve, which can be used in future tool and cap design, is attempted".

## 1.2 APPROACH

To be able to achieve the above mentioned a literature study is performed followed by experiments.

At first more knowledge about cemented carbides was needed because the regular material science course at the 'Utrecht University of Applied Sciences' does not go in detail about these materials. After that, a literature study was performed on the wear and failure of cemented carbides. Being in use in a process environment, especially the failure of the cemented carbide tooling due to fatigue was investigated. Soon was discovered that more knowledge about fracture mechanics was needed to understand the literature about fatigue behavior of cemented carbides.

By using the obtained knowledge of fracture mechanics, the literature study on the fatigue behavior is continued. After this study all knowledge obtained during these literature studies is summarized resulting in the first part of this thesis.

The next step was to state one or more hypothesis and to design a test to verify these. This next phase resulted in the second part of this thesis.

### 1.3 OUTLINE

This thesis is structured as follows. In chapter 2 some general information about cemented carbides is given. This information helps the understanding of the different behavior of cemented carbides if compared to steel. According to Torres et al. [8], “Linear Elastic Fracture Mechanics (LEFM) represents a quite effective approach for rationalizing the fracture behavior of cemented carbides”. This is why in chapter 3 some elementary fracture mechanics is explained. Furthermore in chapter 3 transverse rupture strength is explained because according to Ferreira et al. [17] “fatigue initiation of inherent defects is predominant over propagation”.

In chapter 4 fatigue is covered. Fatigue behavior is broken down in three stages. The most important stages are stage I, fatigue crack initiation and stage II, fatigue crack propagation. Because stage I is rather empirical this is not explained further. Stage II can be described with LEFM and is covered more widely.

To be able to compare the effect of different machining methods and environmental conditions on crack initiation a test is designed. This test setup can be found in chapter 5. The results of this test are also presented in chapter 5.

In chapter 6 the results are summarized and the conclusions are presented. Recommendations for future, complementary investigations are given in chapter 7.

Every chapter starts with an introduction in which is explained why the chapter’s topic is covered. In every introduction a part of Figure 1-2 is displayed to show the relation of the chapter to the general study.

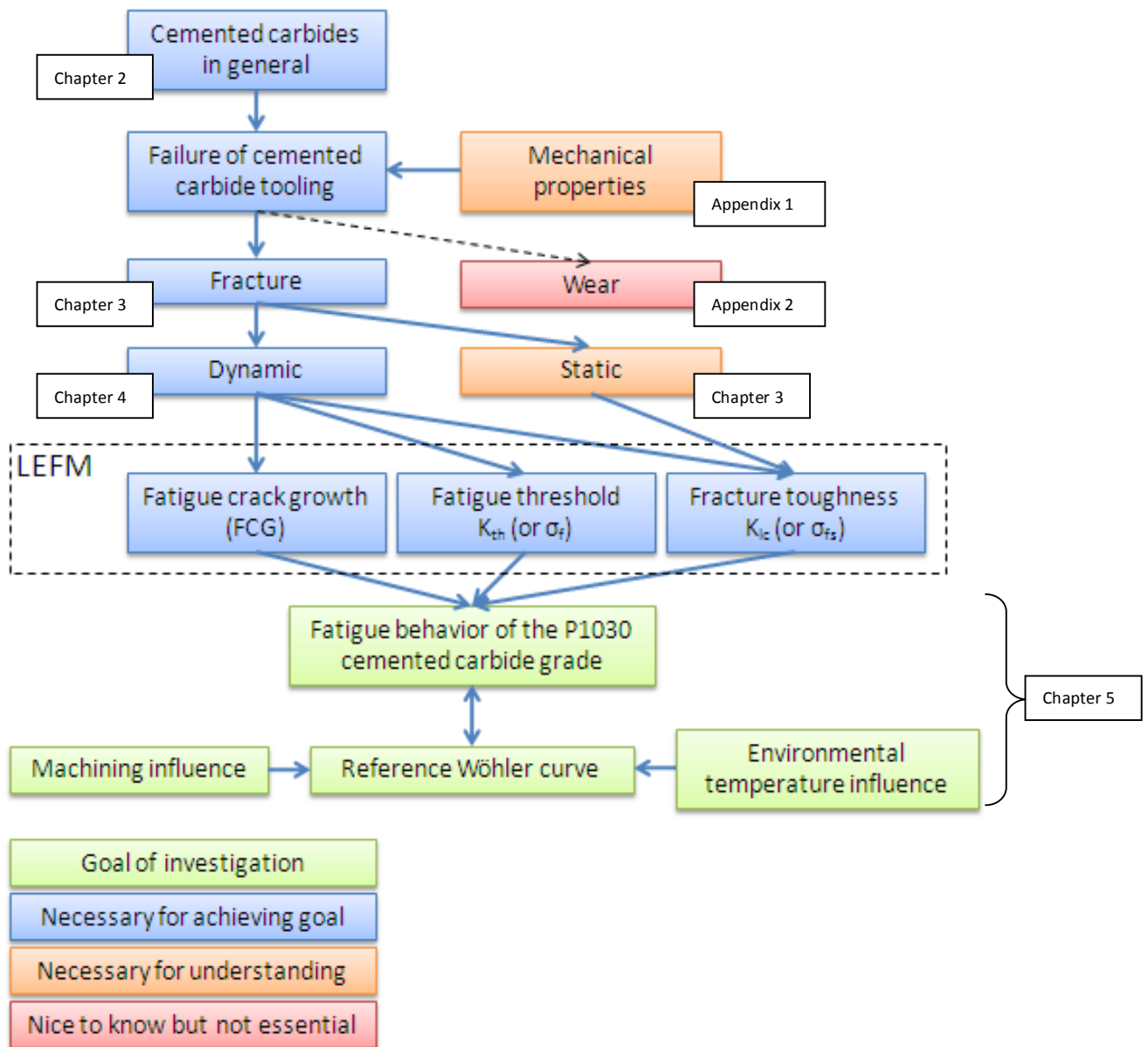
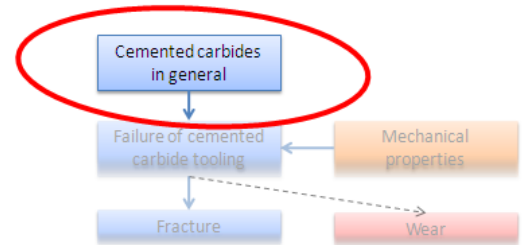


Figure 1-2 Thesis outline explanation

## 2. CEMENTED CARBIDES

Cemented carbides are widely used materials for tools, structural components and wear parts. They exhibit an exceptional combination of strength, toughness and wear resistance as a result of the extremely different properties of their two interpenetrating constitutive phases [15]. For understanding their fatigue behavior, this chapter covers some general (background) information about cemented carbides.



### 2.1 HISTORY

The initial development of cemented carbides, also called hard metal or tungsten carbide, occurred in the early 20<sup>th</sup> century in Germany. It was found while looking for an alternative to diamond used in dies for wire drawing of tungsten.

The commercial use of cemented carbides began in 1927 with a brand called Widia, coming from the German phrase “wie Diamant” (like diamond), referring to the material’s hardness. At first it was primarily used in the mining and timber industry. Because of their high hardness, compressive strength and abrasion resistance they were especially suitable for drilling and sawing. But since the sixties it is also successfully applied in the metal industry as tooling material for extruding, deep-drawing and blanking metal. Also in other sectors, in which tooling wear was high, cemented carbides are nowadays widely applied. [1]

### 2.2 WHAT ARE CEMENTED CARBIDES?

Cemented carbides are composite engineering materials with a unique combination of strength and hardness. Cemented carbides are a range of materials which consist of hard and brittle carbide particles bonded together by a ductile metallic binder, a so called metal matrix composite.

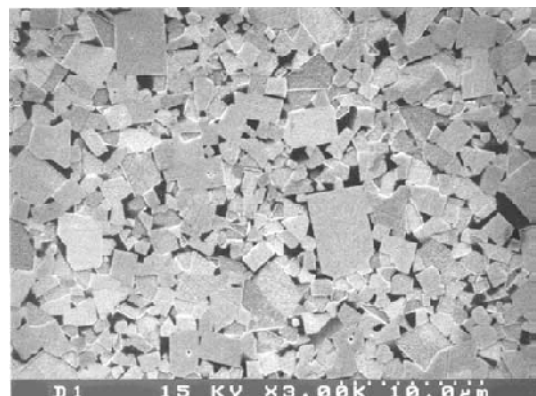
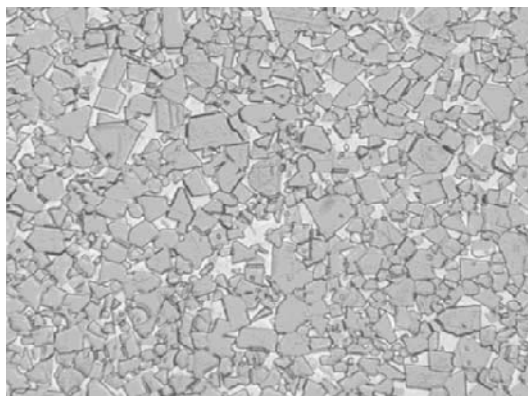


Figure 2-1 WC-Co microstructure examined by optical (left) and scanning electron (right) microscope [2]

Tungsten carbide (WC), together with cobalt (Co), forms the basic cemented carbide structure from which other types of cemented carbides have been developed. Those cemented carbides can contain various proportions of titanium carbide (TiC), tantalum carbide (TaC) and niobium carbide (NbC). Also cemented carbides are produced which have the cobalt binder phase alloyed with, or completely replaced by, other metals such as iron (Fe), chromium (Cr), nickel (Ni), molybdenum (Mo) or alloys of these elements. These modifications to its composition are done to change physical and chemical properties to ensure maximum resistance to wear, deformation, fracture, corrosion and oxidation.

Philips P1030 is a cemented carbide grade containing only tungsten carbides and cobalt. This cemented carbides grade is the main subject of interest of this paper. Grades likes this are classified by their binder content and carbide grain size. Those two parameters greatly determine the physical properties of the cemented carbides and their most appropriate application.

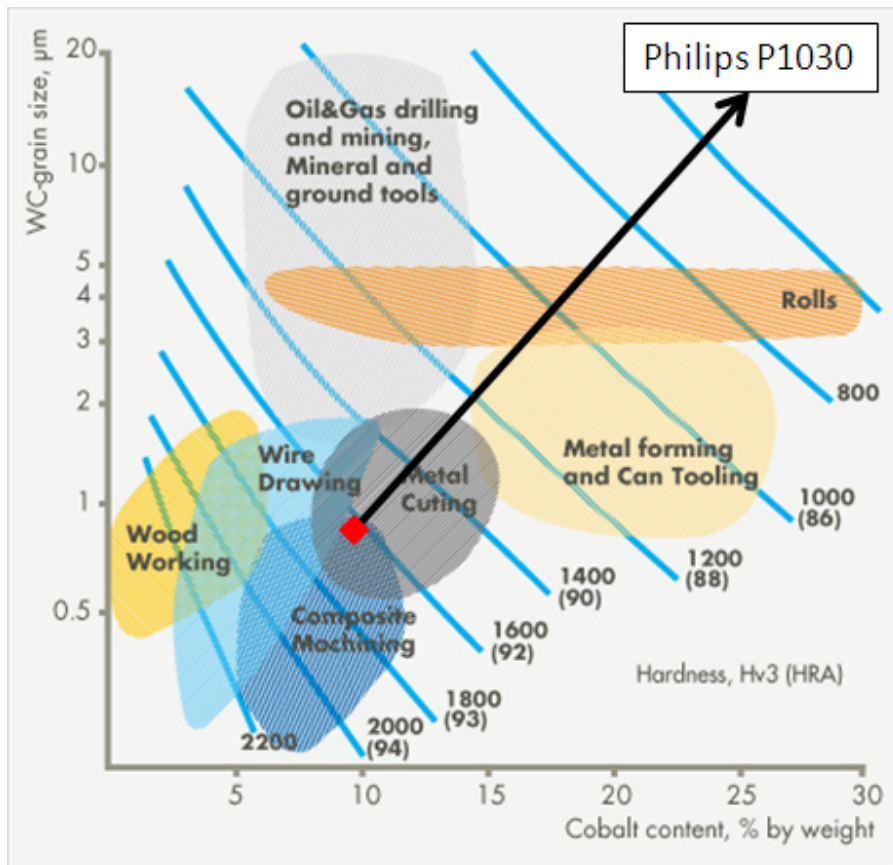


Figure 2-2 Application range of straight grade cemented carbide [3]

## 2.3 HOW IS IT MADE?

Cemented carbides are powder metallurgical materials. This means that this material is not casted into shape but prepared by a sinter / sinterHIP process.

This process begins with the creation of tungsten carbides by carburizing tungsten with graphite. These tungsten carbides are subsequently milled and selected by grain size. The selected carbides are then mixed with cobalt powder to acquire the desired mixture. This mixture is milled, dried and compacted into a form. This form can be machined relatively easy into a desired shape by diamond tooling.

This desired shape is subsequently sintered in a furnace at about 1450°C, just above the melting point of cobalt. This enables the molten cobalt binder to combine with the tungsten carbides. Sintering can be done with or without hot isostatic gas pressure (HIP).

During this heat treatment all present pores are filled with liquid cobalt, resulting in volume shrinkage of the blank of about 50%. After sintering / sinterHIP'ing the blanks are slowly cooled (to prevent origination of residual, thermal induced, stresses) resulting in tungsten carbide grains fixed in a solidified cobalt binder matrix.

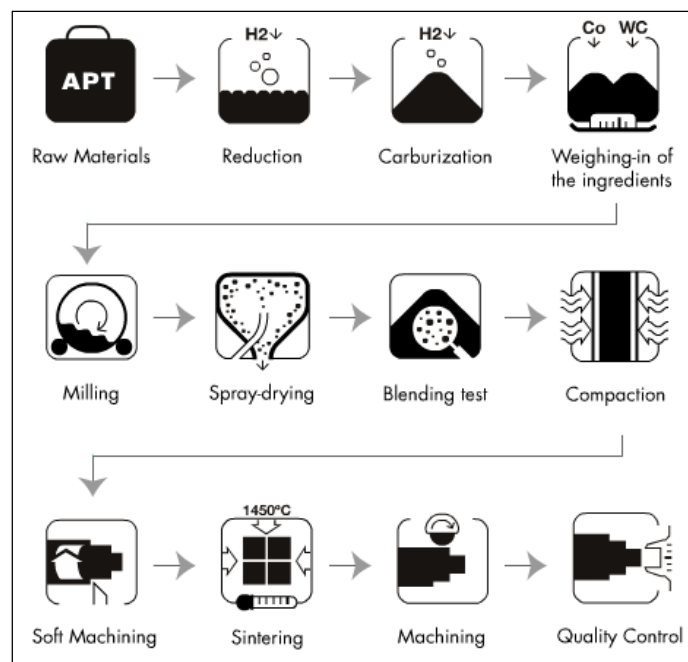
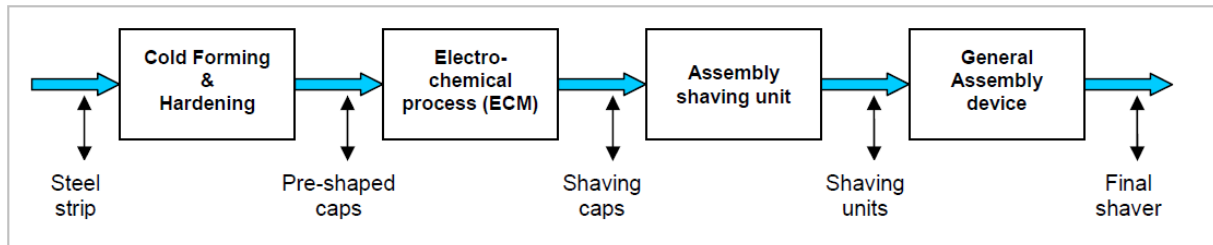


Figure 2-3 Cemented carbide production process [3]

## 2.4 CEMENTED CARBIDES IN SHAVING CAP PRODUCTION

Shaving performance is mostly determined by the shaving cap and cutter. The production process of the shaving cap from strip to shaver is shown below:



The cold forming process consists of multiple steps like deep drawing, blanking and cutting. Due to the tough nature of the strip material high forces are necessary to create the shaving caps. Also to keep the cost price of the shaving caps as low as possible, long tool life is demanded so wear should be avoided as much as possible.

The high abrasion resistance and compressive strength makes cemented carbide a suitable material for tooling in these processes.

## 2.5 FLATTENING OF THE RUNNING GROOVE

One process step in cold forming a shaving cap is flattening the running groove. In this step the shape of the running groove is accurately determined and the bottom thickness is reduced. This process step requires the highest forces and thus generates the highest stresses in the punch and ejector.

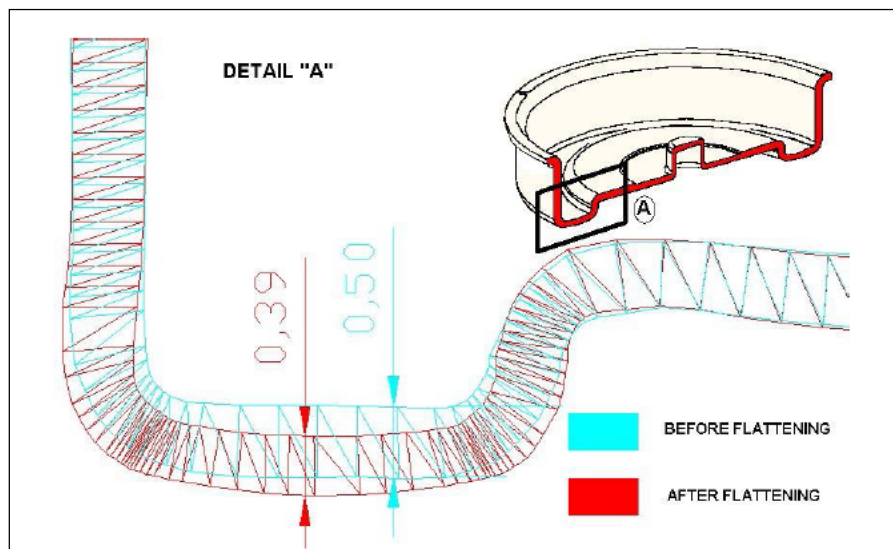


Figure 2-4 Flattening the running groove

To be able to withstand those high forces and induced stresses a special designed cemented carbide grade is used as tooling material for the punch and ejector; P1030. P1030 is an internal code which corresponds to materials available at a number of suppliers. (see appendix 7 for a table with the suppliers own codes)

The material properties of the P1030 grade are shown below (see appendix 8 for P1030 standard):

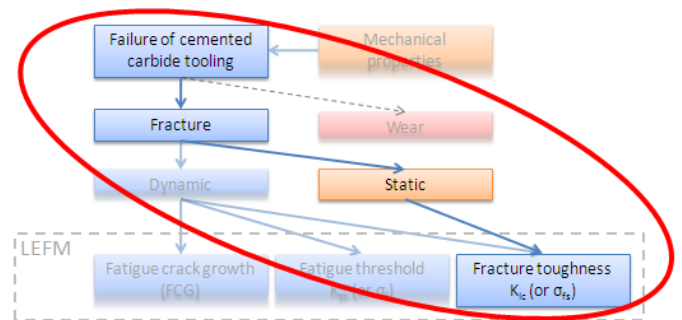
Internal code	P1030
Grade	Co9-F
Grain size [ $\mu\text{m}$ ]	0,8-1,3
Wt.% Co	8-10
Hardness [HV30]	1550
Flexural strength ( $\sigma_{fs}$ ) [GPa]	3,0
Compressive strength ( $\sigma_p$ ) [GPa]	5,9
Young's modulus (E) [GPa]	580
Poisson's ratio ( $\nu$ ) [-]	0,23
Palmqvist toughness (WK) [kJ / m]	Min. 700
Density ( $\rho$ ) [g / cm <sup>3</sup> ]	14,5
Specific heat (C) [J / (kg * K)]	210
Thermal conductivity ( $\lambda$ ) [W / (m * K)]	75
Linear coefficient of expansion ( $\alpha$ ) [ $10^{-6}$ / K]	5,5
Resistivity [ $10^{-8}$ $\Omega$ * m]	19

In the appendix more about some key material properties is explained. Knowledge about these properties is necessary to understand the failure of cemented carbides.



### 3. FRACTURE

The fatigue behavior of cemented carbides can be described by Linear Elastic Fracture Mechanics (LEFM) according to Torres et al. [8]. This chapter covers the static part of fracture and explains the basics of LEFM. This basic knowledge is needed to understand the literature about fatigue behavior of cemented carbides.



#### 3.1 INTRODUCTION

Beside wear, also fracture limits usability of the tooling in cold forming processes. Fracture is defined as the separation of a body into two or more pieces in response to an imposed stress at a temperature level significantly lower than the melting temperature of the material.

#### 3.2 DUCTILE VERSUS BRITTLE

Two fracture modes are discerned in engineering materials: ductile and brittle. The difference between these modes is based on the material's ability to experience plastic strain. Ductile materials exhibit significant plastic deformation before fracture. Brittle materials, in contrast, exhibit little or no plastic deformation before fracture occurs. The difference in this is determined by the ability of a material to absorb energy; high absorption leads to ductile fracture and, vice versa, low absorption leads to brittle fracture.

Both fracture modes show specified types of fracture surfaces/profiles. Highly ductile fracture will result in a necked specimen (Figure 3-1a) and moderately ductile fracture will show a necked specimen with a part of the surface perpendicular to the tensile direction and a part of the surface with a 45° angle relative to the tensile direction (Figure 3-1b). Pure brittle fracture will result in a flat fracture surface perpendicular to the tensile direction (Figure 3-1c).

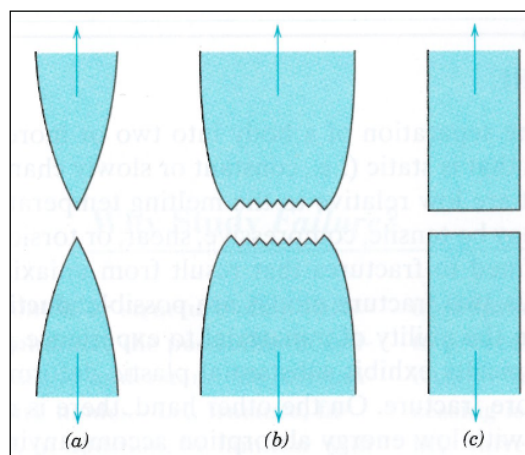


Figure 3-1 Fracture profiles [6]

### Ductile to brittle transition

Ductile and brittle are relative terms; a fracture may be one or the other depending on the situation. Ductility is defined as the percent elongation and/or reduction in area of the material and is a function of the temperature, strain rate and stress state. A change in these parameters makes it possible for ductile materials to fracture in a brittle way. For temperature this is explained as follows [7]:

Brittle fracture, due to splitting of the material, occurs when the (tensile) splitting strength (splijtsterkte) is exceeded. Ductile fracture, due to shear, occurs when the shear strength is exceeded. For steel, the splitting strength is independent of the temperature. Shear strength does show dependence; shear strength decreases with increasing temperature. So for low temperature values the splitting strength is lower than the shear strength resulting in brittle fracture. At higher temperature values, right of intersection  $S_1$  (Figure 3-2), shear strength is lower than the splitting strength resulting in ductile fracture.

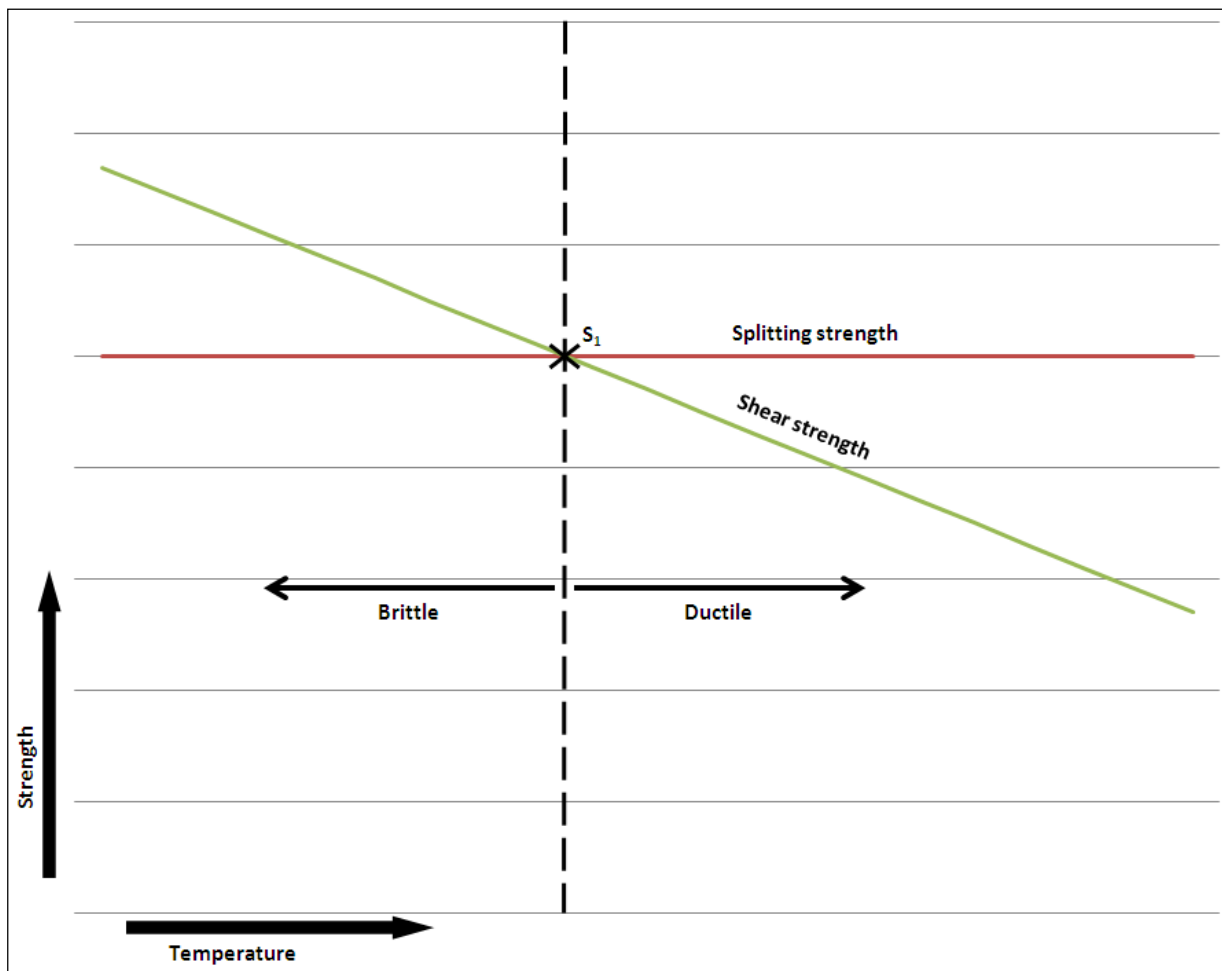


Figure 3-2 Ductile to brittle transition

### 3.3 BRITTLE FRACTURE

As earlier mentioned, brittle fracture takes place without any noticeable deformation and by rapid crack growth. The motion of crack growth is perpendicular to the direction of the applied tensile stress resulting in a flat fracture surface. For very hard and fine grained brittle materials, such as cemented carbides, these surfaces will not show a discernable fracture pattern. According to Y. Torres et al. [8] fracture of the very hard carbide particles in cemented carbides will not occur because the softer, more ductile, cobalt binder will fail first resulting in an intergranular fracture (see Figure 3-3).

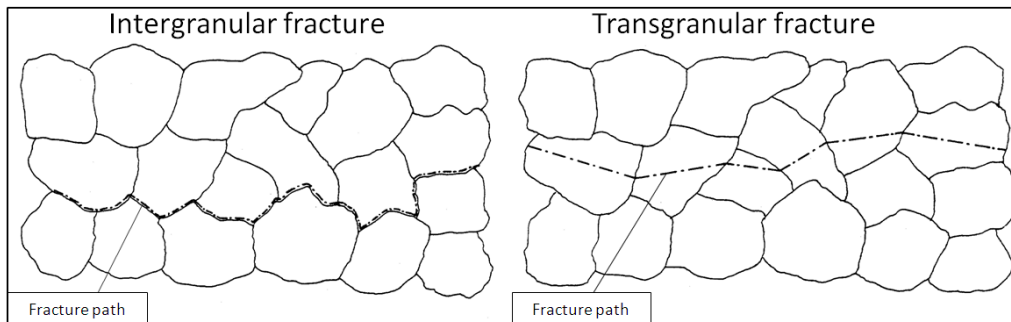


Figure 3-3 Fracture types [7]

### 3.4 LINEAR ELASTIC FRACTURE MECHANICS (LEFM)

The measured fracture strengths for most brittle materials are significantly lower than those predicted by theoretical models based on atomic bonding energies. This difference can be explained by the presence of microscopic flaws or cracks that already exist at the surface or inside the body of a material. These very small cracks have a negative influence on the fracture strength of a material because they amplify and/or concentrate the applied stress at the crack tip.

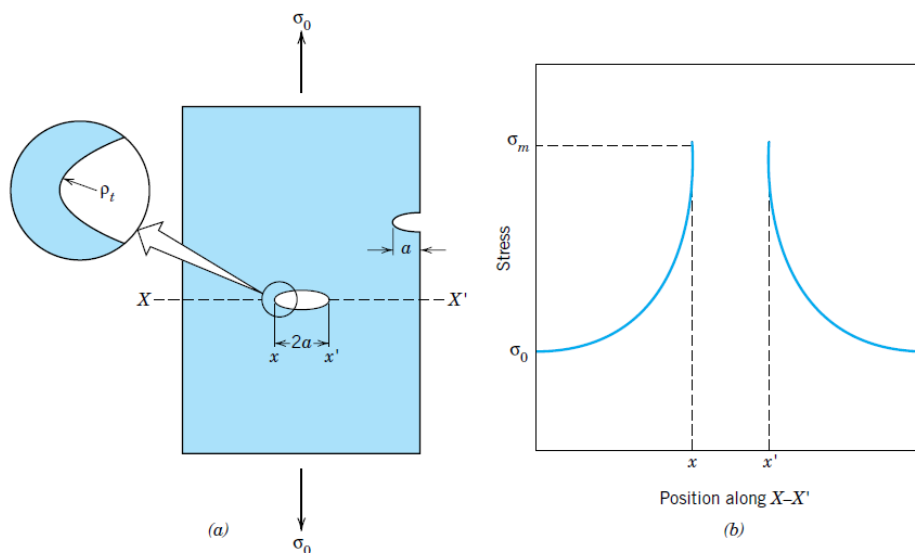


Figure 3-4 (a) Geometry of surface and internal cracks. (b) Schematic stress profile along line X-X' in (a), demonstrating stress amplification at crack tip [6]

According to [6] the maximum stress ( $\sigma_{max}$ ) occurring at the crack tip is:

$$\sigma_{max} = 2\sigma_0 \left( \frac{a}{\rho_t} \right)^{\frac{1}{2}} \quad (1)$$

And the stress concentration factor ( $K_t$ ) is:

$$K_t = \frac{\sigma_{max}}{\sigma_0} \quad (2)$$

Where  $\sigma_0$  is the magnitude of the nominal applied stress,  $\rho_t$  is the radius of curvature of the crack tip and  $a$  is the length of a surface crack or the half length of an internal crack (see Figure 3-4).

The effect of a stress raiser is more significant in brittle than in ductile materials. The reason for this is that ductile materials start to yield at high stress levels. This leads to a more uniform distribution of the stress at the crack tip resulting in lower stress concentration. Yielding is not possible for brittle materials so this effect is not applicable so the theoretical stress concentration will sustain.

According to the principles of fracture mechanics, the critical stress ( $\sigma_c$ ) required for the initiation of crack growth in brittle materials is described by:

$$\sigma_c = \left( \frac{2E\gamma_s}{\pi a} \right)^{\frac{1}{2}} \quad (3)$$

Where  $E$  is the modulus of elasticity,  $\gamma_s$  is the specific surface energy and  $a$  is the half length of an internal crack or the full length of an edge crack.

The equations (1), (2) and (3) are only usable for infinitely large plates. For engineering purposes it is necessary to know the stress concentration in components with finite size.

To be able to compare the performance of hard and brittle materials a beam with an edge crack is used. For such a beam subjected to bending (Figure 3-5) the stress concentration factor at the crack tip is defined by:

$$K_c = Y\sigma_c\sqrt{\pi a} \quad (4)$$

Where  $Y$  is a dimensionless parameter or function depending on both crack specimen size and geometries, as well as the manner of load application. (See [9] for the calculation of  $Y$ )

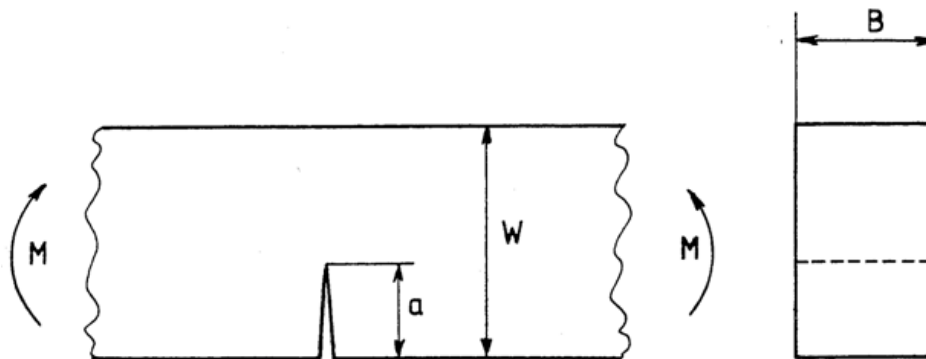


Figure 3-5 Beam with edge crack subjected to bending [7]

The beam in Figure 3-5 is subjected to stress mode I. This stress mode is one of three fundamental stress modes used in fracture mechanics (see Figure 3-6):

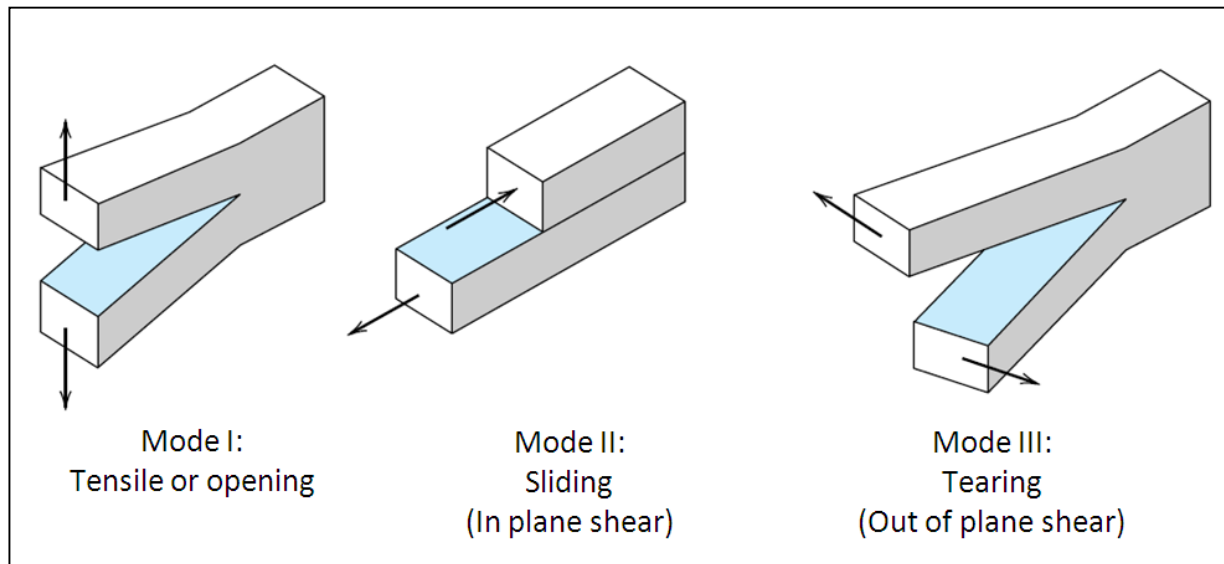


Figure 3-6 Fracture modes I, II and III (where I, II and III are referring to the Roman numbering system) [6]

### Fracture toughness

As can be seen in equation (4) the stress concentration factor is directly proportional to the nominal tension  $\sigma_0$ . At low nominal stress levels there will be no crack propagation but when  $\sigma_0$  is increased a critical  $K$  value will be reached and instable crack growth results. This critical stress intensity factor is called  $K_c$ .

For relatively thin specimens the value of  $K_c$  will depend on the width. When the width increases to a size much greater than the crack dimensions  $K_c$  becomes independent of the specimens width (see Figure 3-7). This state is called 'plane strain' and the critical stress concentration is then denoted by  $K_{Ic}$ , where the subscript I refers to fracture mode I.

$K_{Ic}$  is referred to as the plane strain fracture toughness. It is a fundamental material property and quantifies the materials resistance to brittle fracture when a crack is present. It is defined by:

$$K_{Ic} = Y\sigma_c\sqrt{\pi a} \quad (5)$$

Brittle materials will have low fracture toughness and will show fast, unstable crack growth. It is possible to influence the fracture toughness by changing temperature, strain rate and microstructure.

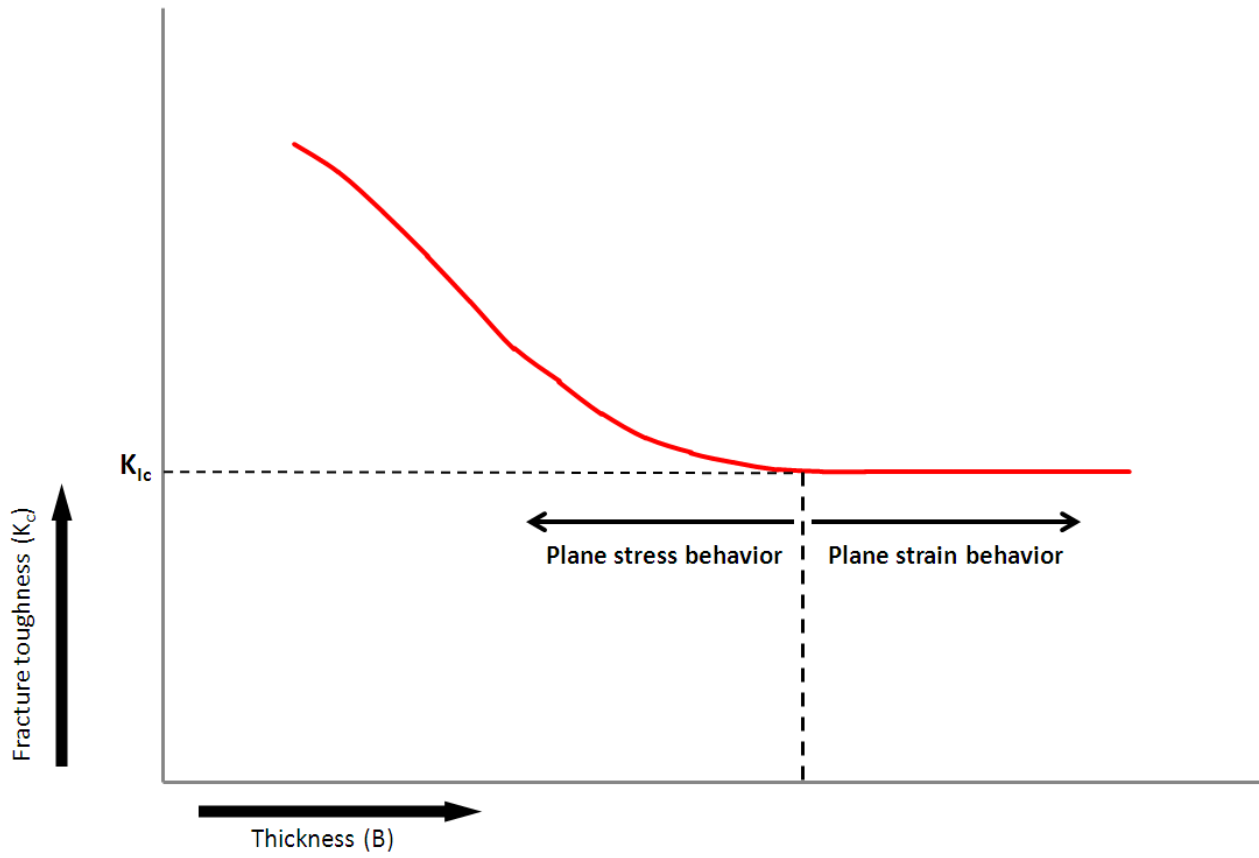


Figure 3-7 Plane stress and plane strain

### 3.5 TRANSVERSE RUPTURE STRENGTH

The relative low scatter of  $K_{Ic}$  makes fracture toughness a useful tool for quality control, materials evaluation and comparison [13]. Unfortunately the  $K_{Ic}$  only says something about the intrinsic strength of a material while the fracture of cemented carbides is dominated by nature and distribution of pre-existing flaws. Furthermore, to calculate the fracture toughness of a material the length of a crack and the crack tip radius should be known. This makes the use of fracture toughness as a parameter to quantify a material's strength not always suitable. The reason for this is that there is no such thing as a flawless surface (see Figure 3-8); even super-finished surfaces do not have a roughness value ( $R_a$ ) of zero. So cracks can initiate from every imperfection of the material's surface depending on the crack tip radius and crack length (see equation 1).

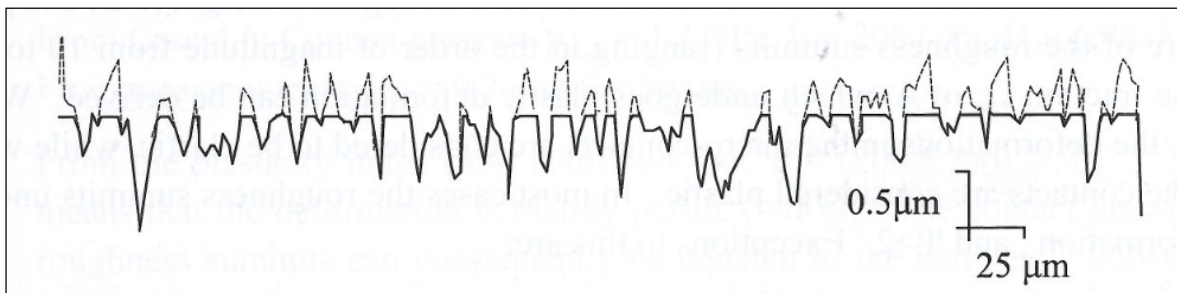


Figure 3-8 Grinded surface given super-finish [4]

Also subsurface imperfections (i.e. cracks and porosities), heterogeneities (ongelijksoortigheden) (see [12]) and internal stresses can noticeable influence the strength of a material. For engineering purposes it is then more convenient to use a 'normal', macro scale, stress-strain parameter, like tensile or yield strength, to quantify a material's strength which is not depending on these micro scale imperfections and, for instance, allowing the discrimination of different machining options.

The stress strain behavior of brittle materials is usually not determined by a tensile test used for most materials. According to [6] the reasons for this are:

- Obtaining specimens with required geometry is very difficult
- Gripping both ends of the specimen firmly without fracturing them is difficult
- Failure of these materials occurs after very little strain (at about 0,1%) which makes it necessary that the specimens are perfectly aligned in the test setup to avoid the presence of bending stresses

Therefore a transverse bending test is used to be able to discern the (macro scale) strength of hard and brittle materials. In this test a beam specimen, shaped rectangular or round, supported at both ends, is subjected to a bending moment by a force applied between the two supports (see Figure 3-9).

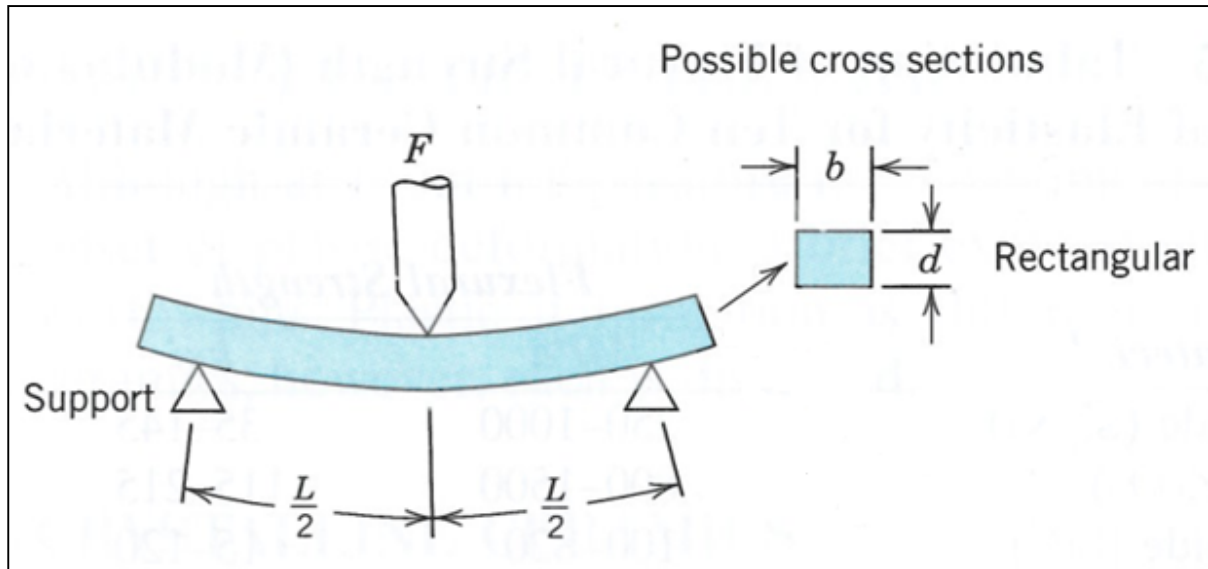


Figure 3-9 Three point bending/flexural test [6]

The top of the specimen, the material is compressed. At the bottom of the specimen a state of tension will be present. The largest tensile stress, in the center of the bottom surface of the beam, can be calculated by:

$$\sigma = \frac{Mc}{I} \quad (6)$$

In which:

$M$  is the maximum bending moment:

$$M = \frac{FL}{4} \quad (7)$$

$c$  is the distance from the center of the specimen to the outer fibers (for a rectangular cross section):

$$c = \frac{d}{2} \quad (8)$$

And  $I$  is the moment of inertia of the beam's cross-section (for a rectangular cross section):

$$I = \frac{bd^3}{12} \quad (9)$$

When inserting (7), (8) and (9) in (6), the following equation is obtained [28]:

$$\sigma = \frac{3FL}{2bd^2} \quad (10)$$

(Note that this equation is only valid for a rectangular cross section)

The in equation (10) calculated stress is referred to as flexural strength ( $\sigma_{fs}$ ), modulus of rupture, fracture strength, bend strength or transverse rupture strength ( $\sigma_{trs}$ ).

Due to the fact that the tensile strengths of brittle materials are usually one-tenth of the compressive strengths and fracture occurs at the face subjected to tension, the flexure test is a reasonable substitute for the tensile test [6]. What should be noted is that since the specimens are subjected to compression and tension, the flexural strength is higher than the tensile fracture strength. This can be explained by the probability of an imperfection the material. If a solid is stressed in a standard tensile test, the amount of material experiencing the highest stress is rather large. Thus also the probability that in this stressed area an imperfection is present is rather large. In a transverse rupture test only the outer most fibers experience the highest stress. The probability that an imperfection is present in this very small area is thus also a lot smaller [6].

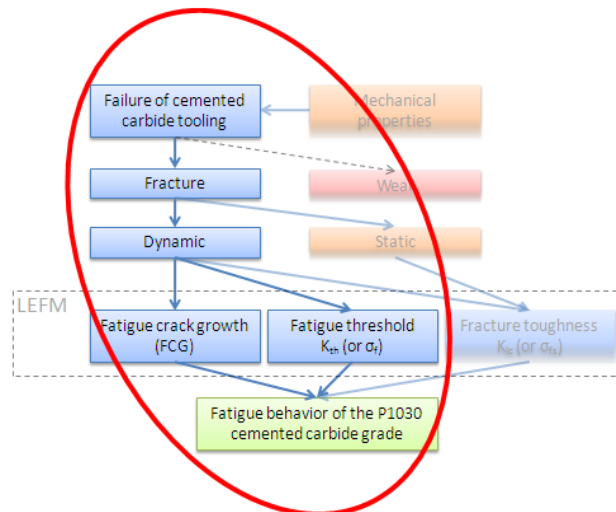


## 4. FATIGUE

Very often materials fail at stress levels considerably lower than the tensile, yield or flexural strength for a static load. Mostly this occurs after a relative long service life in which these materials are subjected to dynamic and fluctuating stresses. This kind of failure is called fatigue.

In this chapter more about fatigue in general and fatigue in cemented carbides is explained. At first some information about fatigue is explained by Wöhler curves. This is subsequently broken down into more detailed fatigue stages, covering crack initiation and crack growth. The breakdown is necessary to understand the literature about fatigue behavior of brittle materials.

Finally some results from the extensive literature study about fatigue behavior of WC-Co cemented carbides are presented. These results are used to generate a test plan that enables comparison of different machining methods and environmental conditions with a reference Wöhler-like curve.



### 4.1 INTRODUCTION

Fatigue is defined by 'the progressive and localized structural damage that occurs when a material is subjected to cyclic loading' [10]. When a material is subjected to a load (below yield strength) it will deform elastically. During this deformation atoms will move to another location [11]. If the load is then removed, the material will assume its original shape but not all atoms will return to their original location. This relocation of atoms results in a change on atomic level and will change the behavior of the material if the load is applied again. Eventually, plastic deformation or generation of small cracks will occur.

## 4.2 FATIGUE IN GENERAL

To understand fatigue, some general fatigue information is needed and described in this paragraph.

The 'dynamic and fluctuating stress' mentioned in the third sentence of this chapter is a general definition of three stress-time modes:

- Reversed stress cycle (Figure 4-1a)  
Amplitude of stress is symmetrical about a mean zero stress level, alternating from a maximum ( $\sigma_{max}$ ; tensile) to a minimum ( $\sigma_{min}$ ; compressive) stress level of equal magnitude and frequency.
- Repeated stress cycle (Figure 4-1b)  
Amplitudes of stress cycle are asymmetrical relative to the zero stress level but with equal frequency.
- Random stress cycle (Figure 4-1c)  
Amplitude and frequency of stress levels vary randomly.

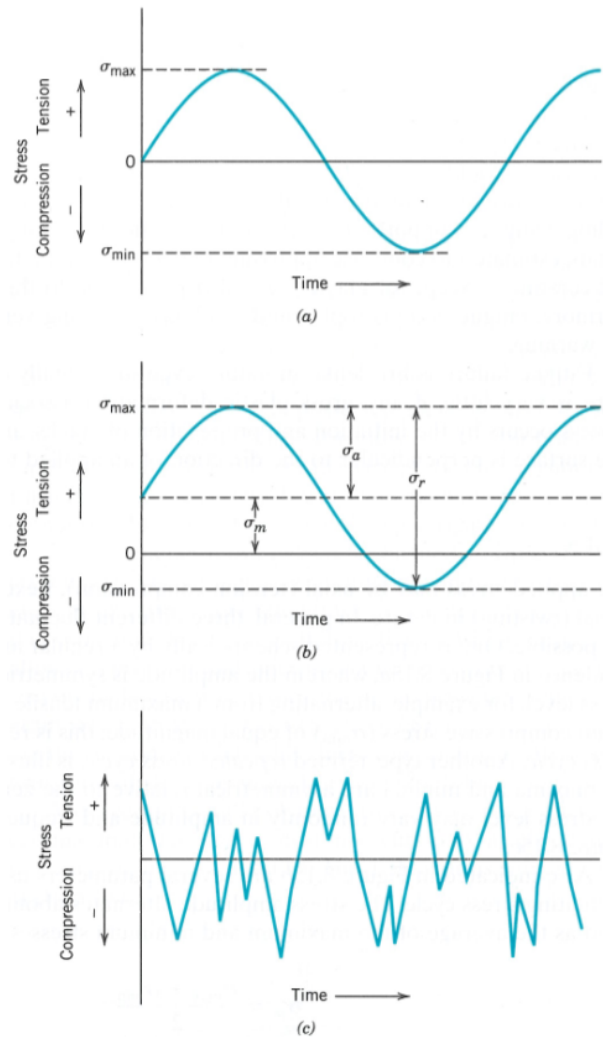


Figure 4-1 Stress-time modes [6]

Test data of fatigue tests is usually plotted as so called 'Wöhler' or ' $S - N$ ' curves. In these curves the maximum stress level ( $S$ ) is plotted versus the logarithm of the number of cycles ( $N$ ) required for failure of the specimen.

The general fatigue behavior of materials, according to [6] can be described as: "the higher the magnitude of stress, the smaller the number of cycles the material is capable of sustaining before failure".

Also according to [6] two types of fatigue behavior can be discerned. The first one is that, for ferrous materials, the  $S - N$  curve becomes horizontal at higher  $N$  values, implicating that there is a stress level at which below materials will never fail regardless of the number of cycles (see Figure 4-2a). This stress level is called the fatigue

limit ( $\sigma_f$ ) or endurance limit. The second type of behavior is that, for most non-ferrous materials, there is no fatigue limit. The  $S - N$  curve continues a downwards trend at increasing number of cycles ultimately resulting in failure regardless of the stress level (see Figure 4-2b). For these kind of materials (i.e. aluminum alloys) the fatigue behavior is defined by the fatigue strength, the stress level at which failure will occur after a specified (mostly  $10^7$ ) number of cycles.

For both types of behavior the fatigue life is defined as the number of cycles at which failure will occur for a specified stress level.

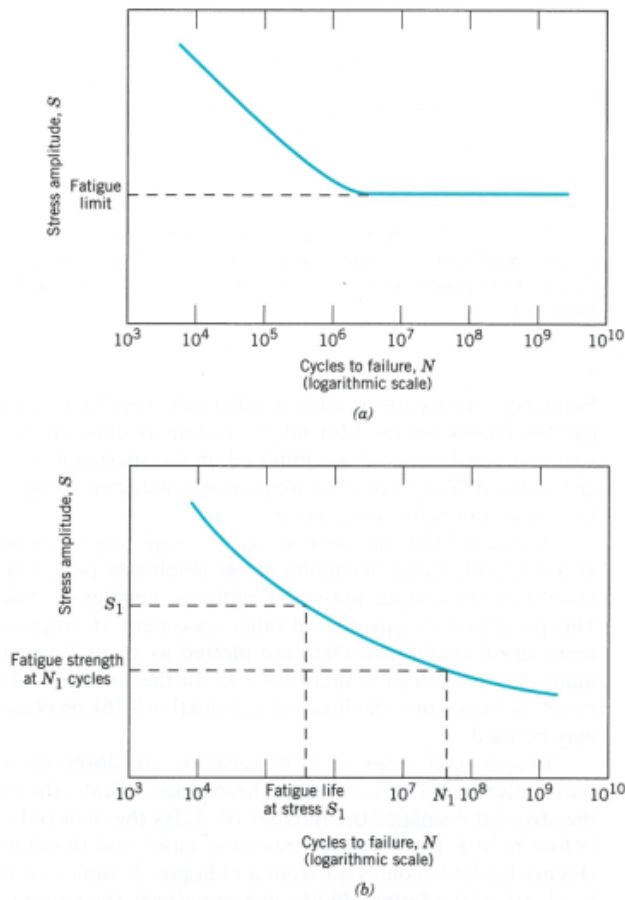


Figure 4-2 S-N curves of two types of fatigue behavior [6] (a) Ferrous (b) Non-ferrous

### 4.3 FATIGUE FAILURE IN STEPS

When examining fatigue in more detail the process of fatigue failure is characterized by three separate steps:

- Crack initiation (formation of small cracks)
- Crack growth (crack propagates with each stress cycle)
- Final failure (rapid failure when crack reaches critical size)

The fatigue life  $N_f$ , defined as the total number of cycles until failure, can be described as follows:

$$N_f = N_i + N_p \quad (11)$$

With  $N_i$  as the number of cycles for initiation and  $N_p$  as the number of cycles for propagation. The final failure occurs so rapidly that it is insignificant to the total fatigue life.

Cracks always initiate at stress concentrations and only initiate when these concentrations rise above a certain threshold stress intensity level  $K_{th}$ . These stress concentrations can be generated by scratches, sharp fillets, material imperfections etcetera. When initiated, slow crack propagation will be present at first. This slow propagation is also referred to as the stage I propagation and is a relative short lived stage.

After this stage, a second propagation stage (stage II) takes over in which the crack growth rate increases substantially. In this stage the direction of crack propagation will change from a random direction into a direction perpendicular to the tensile stress. The surface of a fractured ductile material shows a distinct region of this crack propagation stage with typical markings referred to as 'beachmarks' and 'striations' (see Figure 4-3). At both of these markings it is possible to see the position of the crack tip, which appears as concentric ripples, that expands away from the crack initiation site. 'Beachmarks' and 'striations' differ both in origin and size [6]. 'Beachmarks' are found in components that experienced interruptions during stage II propagation (i.e. a machine only operated in a limited time frame, period after period) making it able to observe them by eye without magnification. 'Striations' represent the progression of a crack front during a single load cycle and can be visualized in an electron microscope. Thus it is possible that there are a huge number of 'striations' between two 'beachmarks'.

Mostly it is possible to analyze the cause of failure by inspecting the fracture surface. The presence of these two types of ripples leads to the conclusion that the failure occurred due to fatigue, but the absence does not exclude fatigue as the reason for failure.

When the crack in stage II reaches a certain depth  $a$  the critical fracture toughness will be exceeded, see equation (4), resulting in fast and unstable crack growth and, finally, full fracture. This final stage leading to fracture is referred to as stage III.

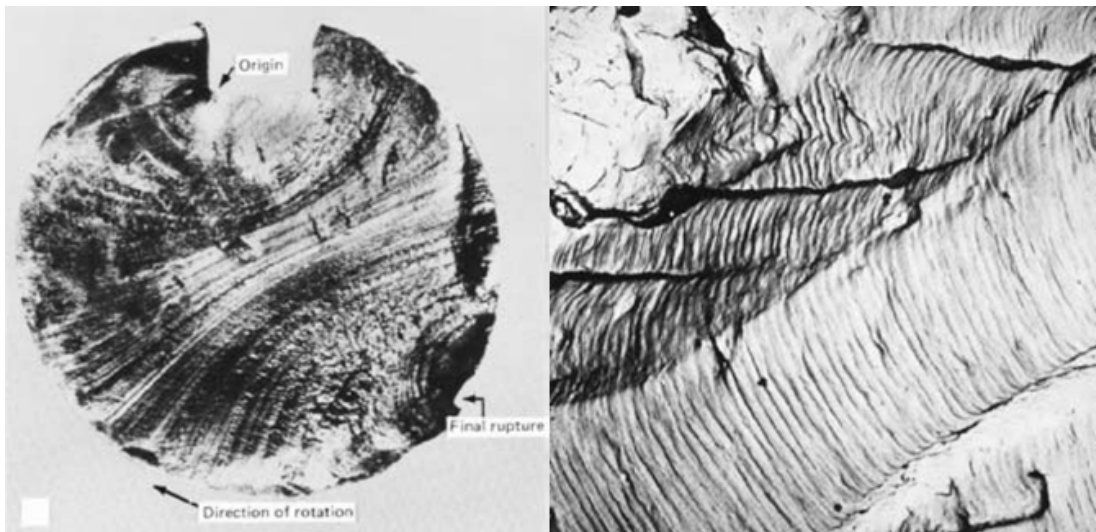


Figure 4-3 Beachmarks (left) and striations (right) [6]

#### 4.4 CRACK PROPAGATION RATE (STAGE II CRACK GROWTH)

According to [6], [7], [8] and multiple other sources, fatigue life ( $N_f$ ) is primarily dominated by the stage II crack propagation referred to as fatigue crack growth (FCG). Especially the amount of crack growth per cycle, the crack growth rate, is important for the fatigue life. In this paragraph crack growth and the crack growth rate are rewritten into an equation usable for calculating the crack propagation part of the fatigue life in equation (4).

##### Crack growth

During stage II propagation cracks grow from microscopic to a critical length. Experiments described by Callister [6] to monitor the crack length during cyclic loading showed that crack length typically develops according the graph below.

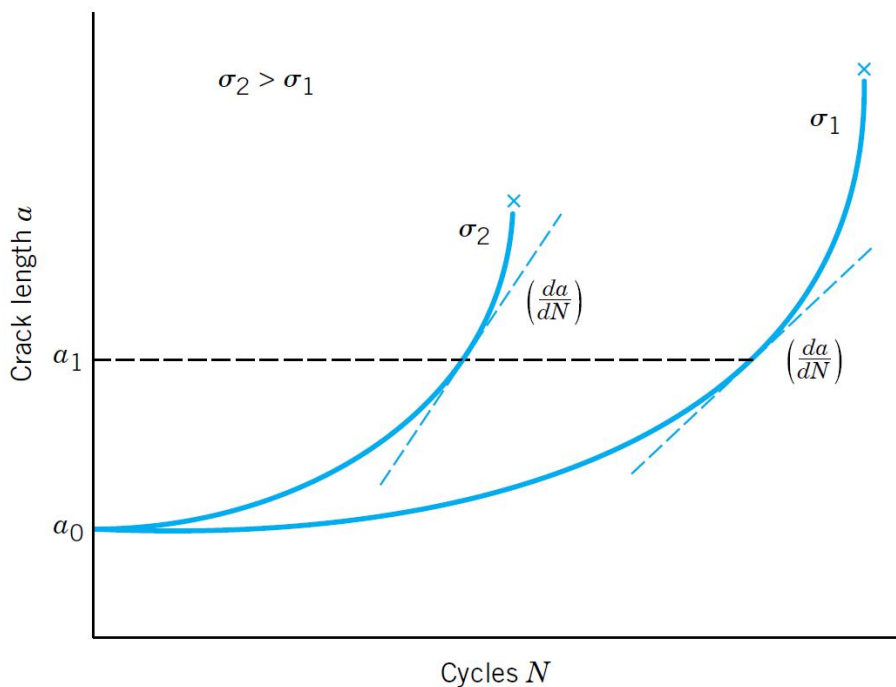


Figure 4-4 Crack length vs number of cycles at two different stress levels [6]

Three important things can be concluded from Figure 4-4:

- 1) Growth rate, defined as  $da/dN$  (the slope of the curve at any point), is initially small but increases with increasing crack size
- 2) Growth rate is increasing with increasing applied stress ( $\sigma_2$  vs  $\sigma_1$ )
- 3) Critical crack size ( $a_c$ ) is earlier reached for higher stress levels (also according to equation (4))

Crack growth in constant amplitude loading cycles, according to [7], is characterized by two parameters:

- Stress intensity factor range:  $\Delta K = K_{max} - K_{min} = Y(\sigma_{max} - \sigma_{min})\sqrt{\pi a}$  (12)  
( $K_{max}$  and  $K_{min}$  are both lower than  $K_c$  or  $K_{Ic}$ )
- Load ratio:  $R = K_{min}/K_{max}$  (13a) or  $R = \sigma_{min}/\sigma_{max}$  (13b)

During the compressive portion of the stress cycle crack growth is equal to zero or negligible.  $\sigma_{min}$  and  $K_{min}$ , being the compressive portion of the stress cycle, can then be taken as zero. Subsequently this means that  $\Delta K$  can then be taken as  $K_{max}$  and  $\Delta\sigma$  as  $\sigma_{max}$ .

### Crack growth rate

The crack growth rate is primarily depending on the stress intensity factor range  $\Delta K$  according to [6], [7], [8] and multiple other sources. Paris [14] derived a relationship that covers this dependence by plotting  $da/dN$  and  $\Delta K$  on a double log paper (see Figure 4-5) resulting in the following equation (which is only valid for the stage II FCG):

$$\frac{da}{dN} = C(\Delta K)^m \quad (14)$$

In this equation parameters  $C$  and  $m$  are material constants which should be gathered from test data.

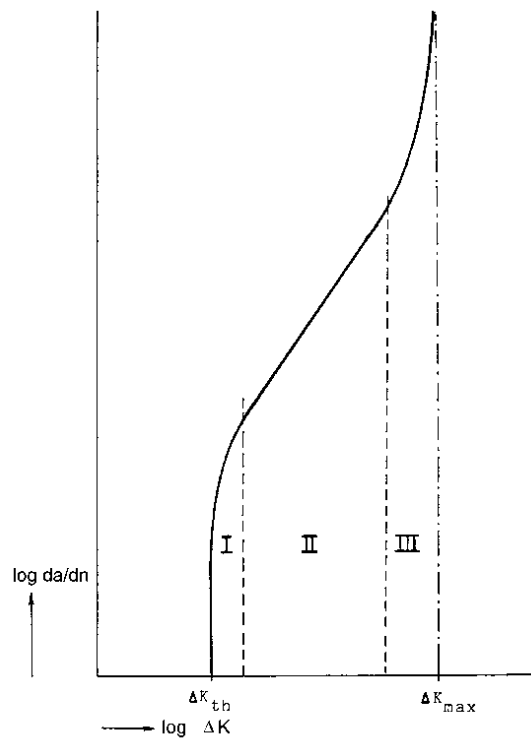


Figure 4-5 Crack growth per cycle as a function of  $\Delta K$  [7]

The curve in region II is essentially linear. This can be verified by taking the logarithm of both sides of equation (14) leading to:

$$\log\left(\frac{da}{dN}\right) = \log(C(\Delta K)^m) \quad (15)$$

$$\log\left(\frac{da}{dN}\right) = m \log \Delta K + \log C \quad (16)$$

Equation (16) is a straight line with slope  $m$  and intercept (snijpunt met y-as)  $\log C$ .

### Stage II fatigue life prediction

If equation (14) is rewritten, it is possible to integrate it and get a value of the predicted fatigue life:

$$dN = \frac{da}{C(\Delta K)^m} \quad (17)$$

$$N_p = \int_0^{N_p} dN = \int_{a_0}^{a_c} \frac{da}{C(\Delta K)^m} \quad (18)$$

In which  $a_0$  is the initial flaw length and  $a_c$  is the critical flaw length. The latter can be determined in fracture toughness tests.

When inserting equation (12) into equation (18) the following equation is obtained:

$$N_p = \int_{a_0}^{a_c} \frac{da}{C(Y\Delta\sigma\sqrt{\pi a})^m} = \frac{1}{C\pi^{m/2}(\Delta\sigma)^m} \int_{a_0}^{a_c} \frac{da}{Y^m a^{m/2}} \quad (19)$$

Assumed is that  $\Delta\sigma$  is constant and that  $Y$  depends on the crack length  $a$  so it can't be removed from within the integral.

Equation (11) is now partly filled but still very difficult to solve:  $N_p$  is difficult to calculate because of dependent variable  $Y$  in the equation and  $N_i$ , which will be very small for most materials but nonetheless not equal to zero, is still unknown.

### Extra explanation on the Paris curve (Figure 4-5)

Almost all materials have some surface cracks (i.e. roughness  $\neq 0$ ) so stage I (crack initiation) has already occurred. Furthermore stage III is very short, having almost no effect on the total fatigue life. Due to these two reasons the Paris curve is usually simplified and plotted as shown below.

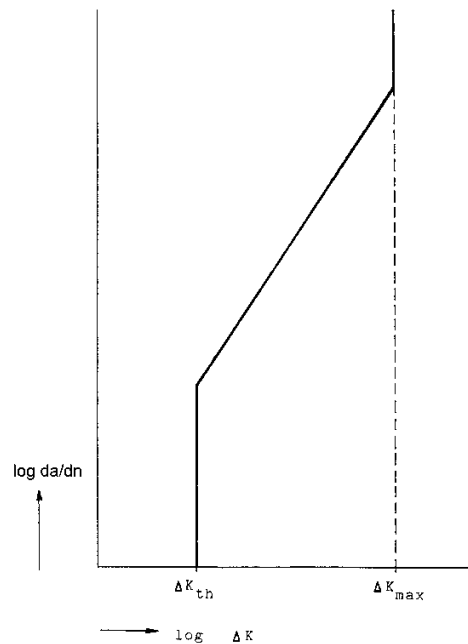


Figure 4-6 Simplified Paris curve [7]

The left side of the curve is confined by  $K_{th}$  or  $\Delta K_{th}$ , the threshold stress intensity factor, the minimum stress required to propagate an existing crack. The right side of the curve is confined by  $K_{Ic}$  or  $\Delta K_{max}$ , the value at which rapid, unstable, crack growth leads to failure (see fracture toughness).

### Crack closure effect

The effective value of  $\Delta K$  is usually a little lower than expected due to the 'Elber-effect'. This is the crack closure effect and can be explained as follows according to [7]:

“At both sides of a crack path plastically deformed zones are present. The crack tip is already in advance of these zones. When the crack is closing these zones do not exactly fit into each other. Consequently the crack has already closed before the stress reaches its minimum level. Only the part of the cycle in which the crack is opened contributes to crack growth resulting in a lower effective value of  $\Delta K$  and a lower crack growth rate ( $da/dN$ ) than expected.”

## 4.5 FATIGUE IN WC-CO CEMENTED CARBIDES

After the literature study performed to get a better understanding on fatigue behavior of materials another literature study is performed to investigate the fatigue behavior of WC-Co cemented carbides. The most interesting results of this literature study are described in this paragraph.

The fatigue behavior of brittle materials is a little different than that of ductile materials because there is little or no elastic deformation before fracture. But, according to a more general study of Torres et al. [8], the fatigue behavior can be described by LEFM (described in paragraph 3.4).

### Origin of fracture

The origins of the fatigue fracture, as in static fracture, are usually subsurface heterogeneities (pores, abnormally large carbides, binderless carbide clusters) or surface imperfections (subcritical cracks) [8] [15]. These heterogeneities and imperfections result in stress concentrations at which a crack will form and/or propagate.

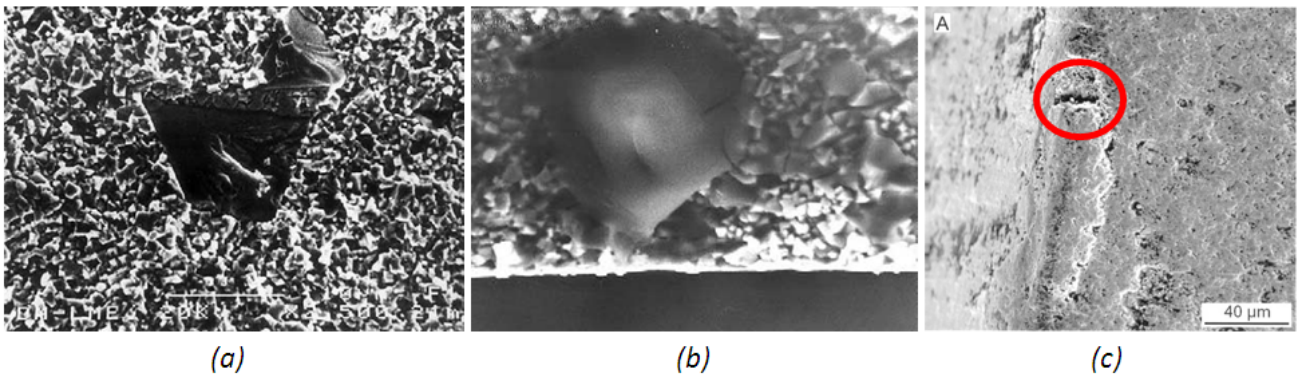


Figure 4-7 Fatigue fracture origins: abnormal large carbide (a), subsurface pore (b) [8] and microcrack (c) [18]

### Determining parameters on FCG

The first thing concluded by Torres et al. [8] about FCG is that there is a very large power law dependence of crack growth rates on  $\Delta K$  and  $K_{max}$ . This means that small differences in applied stress result in relative large fluctuations in the estimated fatigue life making it difficult to implement a damage tolerance analysis for fatigue life prediction.

The second drawn conclusion by Torres et al. [8] on FCG is that there is a 'stress intensity factor range' ( $\Delta K$ ) effect but that the  $K_{max}$  is the dominating parameter determining the fatigue crack growth. Thus the maximum stress in the load cycle is the largest influence on the FCG rate. For the material tested in this study this is clarified by the modified Paris-Erdogan relationship (equation 20) in which  $m$  has a value of 5, and  $n$  has a value of 24:

$$\frac{da}{dN} = C(\Delta K)^m (K_{max})^n \quad (20)$$

The second conclusion is supported by another study of Llanes et al. [15], Torres et al. [16] and Ferreira et al. [17].

Torres' third conclusion in [8] on FCG is that the value of  $K_{th}$  is directly proportional to the load ratio ( $R$ ) implicating that for a given  $K_{max}$ , resistance to FCG initiation increases with a decreasing applied  $\Delta K$ . In other words; if the minimum stress (tensile) comes close to the maximum stress (also tensile) the resistance for crack propagation is higher. For tooling in cold forming processes, at which the minimum stress becomes zero, this means that only  $K_{max}$  will have an influence.

### Microstructural effects

FCG is influenced by microstructural effects according to [15] and [16]. When increasing binder content ( $V_{Co}$ ), mean carbide grain size ( $d_{WC}$ ) or binder mean free path ( $\lambda_{Co}$ ) (see Figure 4-8a), the fracture toughness ( $K_{Ic}$ ) and threshold stress ( $K_{th}$ ) increases, and the FCG rate will decrease. Unfortunately the fracture toughness raises substantially, especially under mode II loading conditions, whilst the other two do not change that significant. This means that the fatigue sensitivity, defined as  $K_{th}/K_{Ic}$ , decreases (see Figure 4-8b).

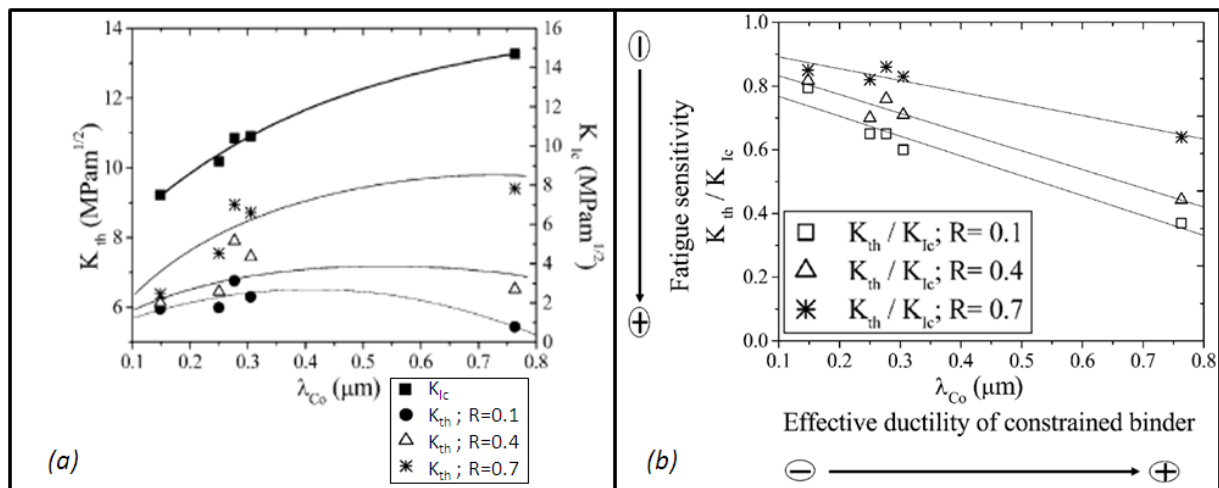


Figure 4-8 Effect of binder mean free path on  $K_{th}$  and  $K_{Ic}$  (a) and on fatigue sensitivity (b) [15]

The increase in  $K_{th}$  and decrease in FCG rate is explained by the increased effective ductility of the binder phase, i.e. when the ductility of this phase is enhanced, better crack tip shielding will be present.

### Frequency dependence

In [19] an investigation on high temperature fatigue behavior of cemented carbides is performed. The test were conducted using to different frequencies, 2 and 22 Hz, both at room temperature and in air. The cemented carbides tested did not exhibit any difference between these tests so frequency independence is concluded.

But another research performed by Evans and Linzer (described by Kindermann et al. [19]), did show frequency dependence. This can possibly be explained by a later paper presented by Pugsley and Sockel [20] in which the corrosion fatigue of cemented carbide tooling is investigated. In this paper frequency dependence is seen when the tooling is subjected to cyclic loads in a corrosive environment. The tests performed in [20] show that if the frequency increases, the fatigue life, in number of cycles, also increases (see Figure 4-9).

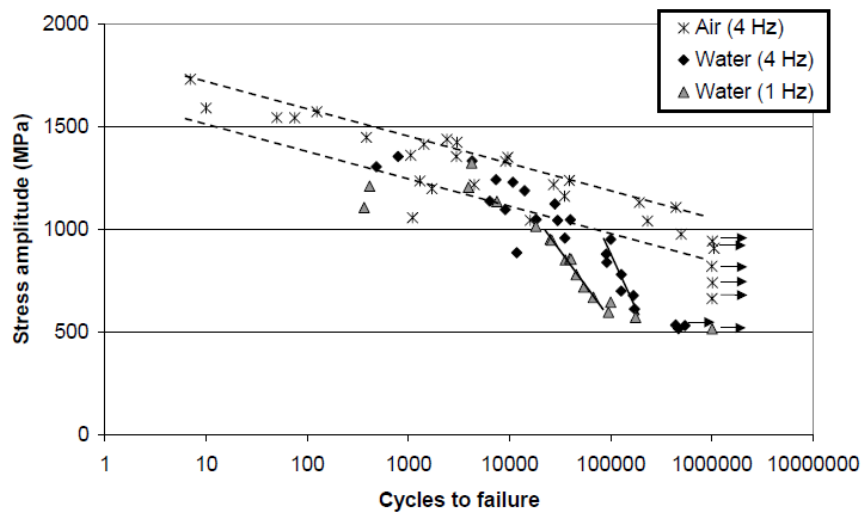


Figure 4-9 WC-Co frequency dependence in corrosive environment [20]

According to ASTM E 647 [21], testing in aggressive and high temperature environments can introduce a significant effect on loading variables such as cycle frequency. The recommendation in this test method is that test should be performed at constant frequency and environment to exclude as much noise as possible.

#### Temperature dependence

An investigation at Philips showed that the required forces, and subsequently stresses, in a cold forming process decrease significantly when the environmental temperature is raised. Consulted literature showed that there is not only a positive effect on the required forces, but also on the fatigue behavior of cemented carbides used for tooling.

In [19] a temperature range between 25°C and 700°C is investigated for a cemented carbide grade with 6wt% cobalt. The universal trend presented in this paper is that the intrinsic material strength ( $K_{Ic}$  or  $\sigma_{fs}$ ) decreases when temperature increases. For very high temperatures (>500°C) also the cyclic strength decreases. Because the slope of the  $S - N$  curves at the high temperatures is equal to the room temperature curves the conclusion is drawn that the loss of strength is not an effect of surface oxidation and surface fatigue, but a true high temperature cyclic effect.

For temperatures around 300°C the inert strength of the material is also lower than for room temperature, but the fatigue strength is, in contrary to the very high temperatures, higher for cycles of thousand and up (intersection of the two curves at thousand cycles) (see Figure 4-10). According to this paper the value of 300°C was the optimum temperature for this grade.

The phenomenon of higher fatigue strength at raised temperatures in [19] is supported by a study at the NPL (UK) performed by Roebuck et al. [22]. In this study an increased fatigue resistance at a temperature level of 300°C is found (see Figure 4-11) for a cemented carbide grade with 10wt% cobalt, comparable to the P1030 grade used for the tooling at Philips.

An explanation on the increased fatigue resistance at elevated temperatures is not given by Roebuck et al. but research performed a year later by Ferreira et al. [17], at a temperature of 500°C, did show comparable results.

There is concluded that this can be explained by the changes in the residual stresses between the carbide and the binder phases and its relationship with subcritical crack initiation.

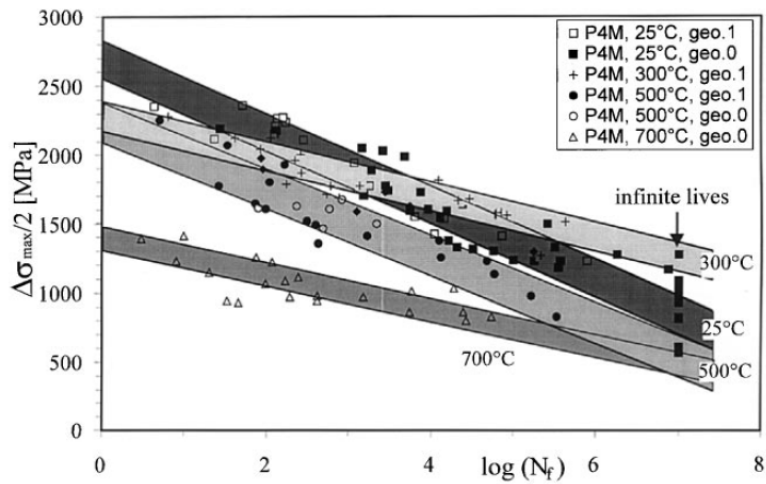


Figure 4-10 Temperature dependence of the cyclic loads of a cemented carbide grade [19]

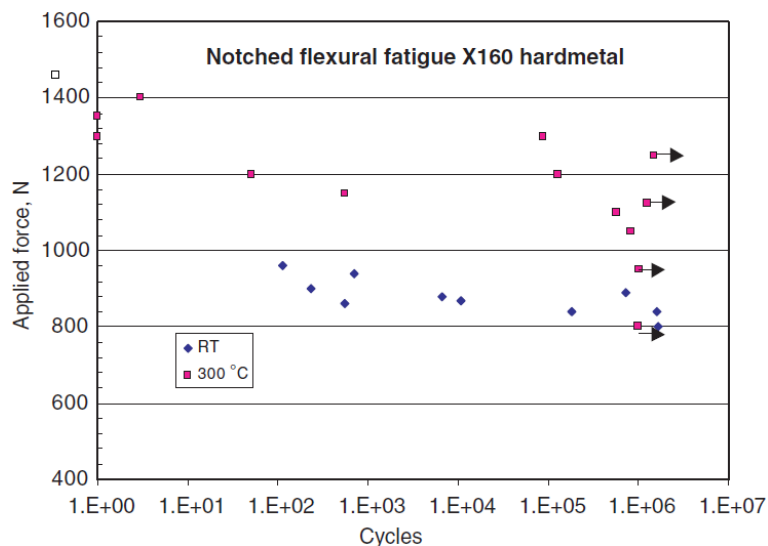


Figure 4-11 Notched flexural fatigue of a cemented carbide grade comparable to P1030 [22]

The reason that an optimum can be found, according to [5], is due to the oxidation effect that will occur if the temperature rises to a level above 540°C (approximate value, will differ per grade). This oxidation will appear as a powder layer or flakes on the surface of the carbide and is abraded away with relative ease.

### Tool production technique effect

Cemented carbide tooling used in cold forming processes is regularly produced by grinding, turning and polishing. These production techniques are able to achieve the very tight specifications on the dimensions required in these processes. Producing relative large surfaces with these techniques is no problem, but if more freedom of shape is demanded other production techniques come into scope.

One of these, non-abrasive, techniques is electrical discharge machining. This technique is increasingly used to overcome technical difficulties and high costs associated with the machining of the hard and brittle cemented carbides.

In [23] research is done on the effect of the EDM production technique on fracture and fatigue behavior of cemented carbides. The general hypotheses, that EDM results in a thermally affected, tensile stress inducing, subsurface zone and poor surface integrity, is tested.

Results in this study show that an EDM'ed specimen shows a flexural strength that is only 45% of that of a polished specimen. To check whether this is due the surface integrity or the thermally affected zone, some specimens are annealed before the test. This annealing step shows a significant increase (70%) in flexural strength compared to the specimen which was only EDM'ed. The flexural strength is even at level of 80% compared to the polished specimen. Therefore the concluded is that the decrease in flexural strength is mostly due to the, EDM induced, residual tensile stresses.

Also the effect on fatigue of the EDM process is investigated. The strength decrease of the EDM'ed specimens is even more pronounced, in terms of fatigue limit and fatigue sensitivity. This is explained by the EDM induced residual stresses which 'imply an additional mean stress; thus, higher effective load ratio at the EDM'ed surface'.

A comparable study performed at the K.U. Leuven [23], comparing different EDM process settings and methods, validates the decrease in flexural strength of wire EDM'ed materials compared to polished specimens. This study also shows that higher flexural strength is achieved when a higher number of EDM finishing cuts are applied. The usage of an oil dielectric results in an even higher flexural strength because the surface of the cemented carbide is less affected by corrosion.

The reason that the grinded specimens show higher flexural strength is explained by Hegeman et al. [24]. In this study, X-ray residual stress measurements are performed. The residual stresses in the grinded surface layer of cemented carbides are found to be compressive (a relation between compressive stress and grinding parameters was not found). These compressive stresses results in a lower effective tensile stress at the outer fibers in a flexural test and thus in higher flexural strength.

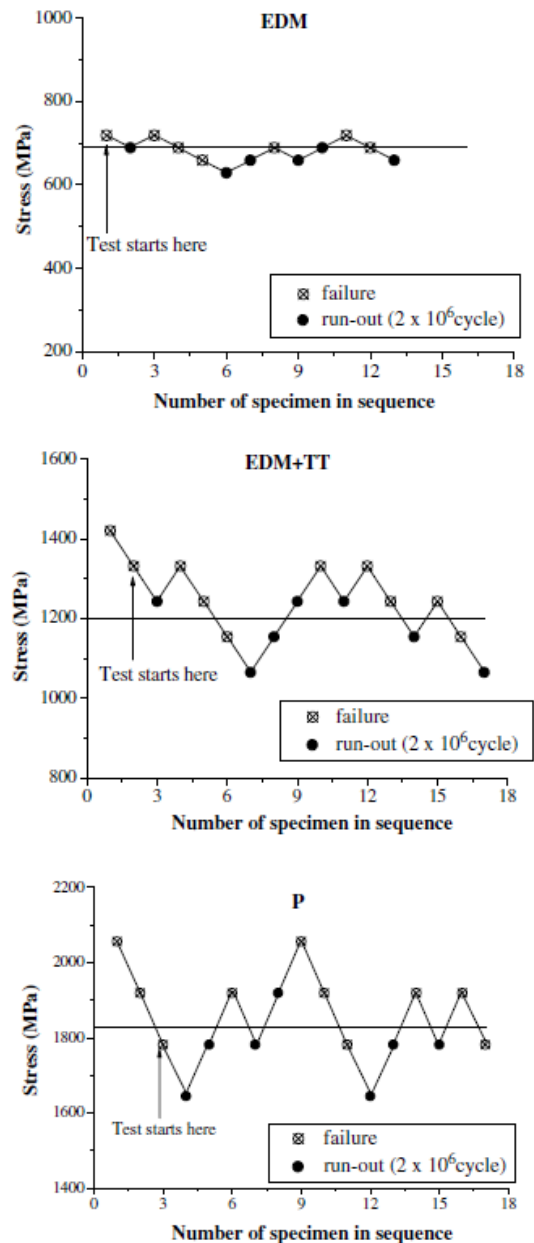


Figure 4-12 Comparison of EDM'ed, EDM + annealed and polished specimens [12]

### Cobalt impregnation

Research performed on the durability of cemented carbide tooling used in the mining industry [25] showed that it is possible to achieve a more cobalt rich outer layer in the tooling, a so called gradient-structure. The benefit of this gradient-structure is that the outer layer, in which the tensile stresses are highest, is enriched with the more ductile cobalt while the main volume of the material is not influenced, keeping the material properties equal. According to [25] this results in an increased ultimate tensile strength and in a two to three times longer fatigue life of the cemented carbide.

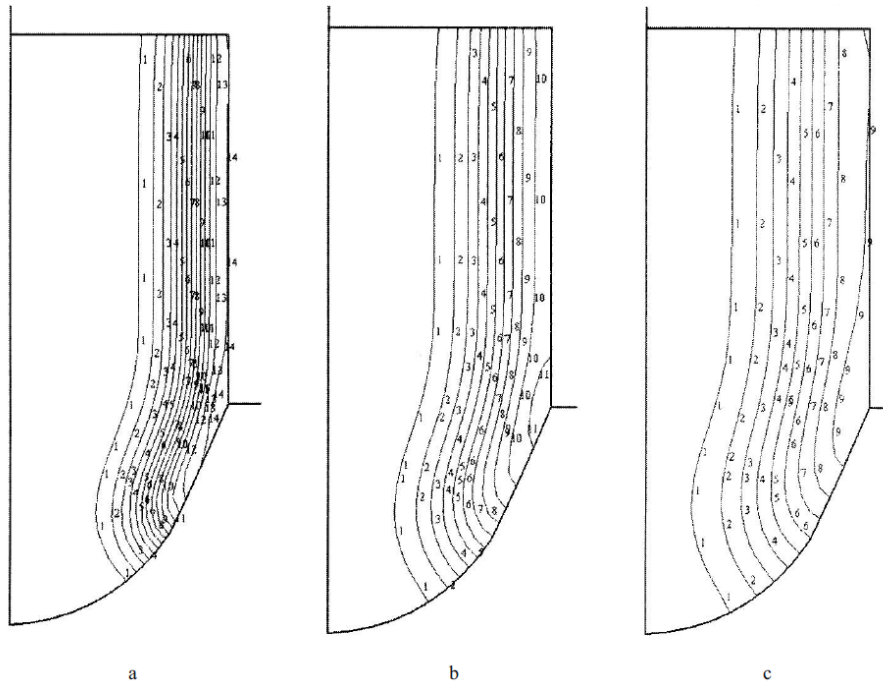
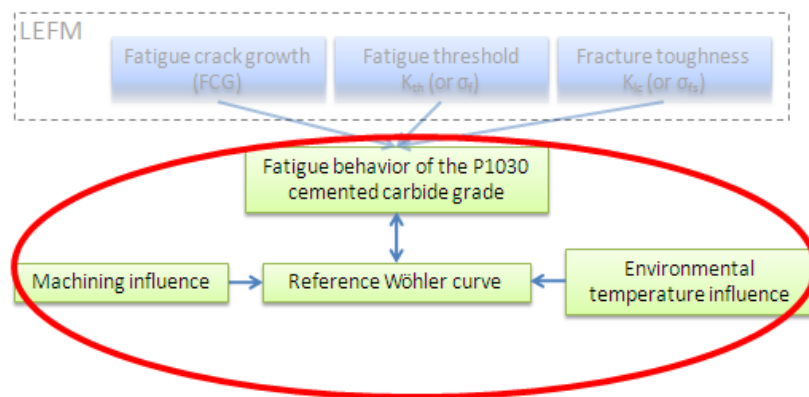


Figure 4-13 Cobalt distribution in WC-Co cemented carbide upon active impregnation of 8s and subsequent holding: (a) 10s, (b) 15s, (c) 20 s. Value of cobalt content (in wt%) is equal to an isoline multiplied by 6 [25].

## 5. TEST SETUP

Literature consulted during this investigation showed that it should be possible to generate a Wöhler-like curve for cemented carbide materials. To verify this, and to generate a Wöhler-like curve for the P1030 cemented carbide grade, a series of test had to be performed. Also the effect of the machining technique is taken into account in the tests. This is done to be able to compare the EDM technique, which allows more freedom of shape, to grinding and polishing, which allows less freedom of shape but will probably result in better tool life. All considerations done before, during and after the test and the results are described in this chapter.



The wish to compare different machining methods results in that working with stress intensity factors is not very practical (more explanation in 5.1). This means that the research performed will be taken one 'abstraction level' higher and that only stress level are compared. The fact that each machining method will introduce specific surface imperfections will be taken as granted.

### 5.1 HYPOTHESIS AND GOAL

#### Wöhler curve

Multiple sources [17, 18, 19, 20, 22, 25] show that it is possible to generate Wöhler-like curves for different types of cemented carbide grades. Unfortunately every grade shows another behavior so for each grade a curve has to be determined. But it should be possible to generate a curve for the P1030 grade used in the cold forming processes at Philips. Expected is that this curve will be starting at a stress level of about 3 GPa (the flexural strength according the material specification, see appendix 6 and 8) and will follow a linear descending trend.

Tooling used in the current processes is grinded and polished, so the reference curve will be generated with polished specimens. Expected is that the fatigue strength, defined as the stress at which the specimens will survive  $10^7$  load cycles, is around 60% of the flexural strength with polished specimens. This level can decrease greatly if the machining technique used to produce the tensile side of the specimen is changed into EDM because of more required freedom of shape. Depending on the EDM process the fatigue strength is expected to be at only 30% if compared to the flexural strength of a polished specimen. A more refined EDM process could result in a higher strength.

As mentioned earlier, a recent, brief research at Philips shows that ‘cold forming at a higher temperature level’ will be of large benefit on the process if more complex forms are desired. This higher temperature level could also be beneficial on tool life according to [17, 19, 22] making it interesting to verify this because also current processes could benefit from this effect. Expected is that the cemented carbide specimens will show a up to 30% higher fatigue strength if the specimens are tested at increased temperature (250-300°C) (see Figure 4-10 and Figure 4-11).

Overall, the Wöhler-like curve and the effects of the increased temperature and machining method are expected to look like the graph in Figure 5-1.



Figure 5-1 Expected test results

Figure 5-1 explained:

Wöhler-like curve and supplementary reference points:

The width of the grey area is not a reflection of the size of the expected spread but only to visualize that spread is expected in the test results.

A number of five specimens will be tested at an equal stress level to be able to indicate the size of the spread and to have a more defined point in the Wöhler-like curve. This more precise determined point is then used to compare the increased temperature and the EDM'ed specimens.

*Increased temperature effect:*

*As can be seen in Figure 4-10 there is an intersection at about  $10^4$  cycles. Before this intersection the required number of cycles for failure at a given force is lower at 300°C than at room temperature. After this intersection the required number of cycles for fracture is higher at increased temperature compared to room temperature. Expected is that this is also valid for P1030.*

*Because of the limited number of specimens and the expected spread in test results it is decided to only create a single point in the Wöhler plot for increased temperature to verify if there is any measurable effect. To be able to see any possible, positive, temperature influence this single point is determined to be at a cycle level of at least  $10^4$  cycles.*

*“Specimens tested at the same stress level but at increased temperature are expected to be able to endure more cycles than the specimens tested at room temperature. Therefore the green dots are displayed right of the blue dots.”*

*EDM effect:*

*Figure 4-12 shows that EDM'ed specimens show considerable lower transverse rupture strength. Therefore it is expected that these specimens will fracture at a very low cycle number compared to the grinded specimens at a certain stress level.*

*“EDM'ed specimens tested at the same stress level are expected to endure significantly less loading cycles than the grinded specimens. Therefore the red dots are displayed left of the blue dots.”*

### Paris curve

The generation of a Paris-like curve will **not** be attempted in the test. This is due to the fact that a Paris curve says something about the intrinsic strength of a material. It also does **not** allow comparison of different machining methods because it is impossible to machine a sharp crack in multiple ways. Furthermore in [17] is stated that “fatigue initiation from inherent defects is predominant over propagation; therefore  $S - N$  results are more adequate”.

### Approach

Before performing the test an approach was defined. This approach is visualized in Figure 5-2.

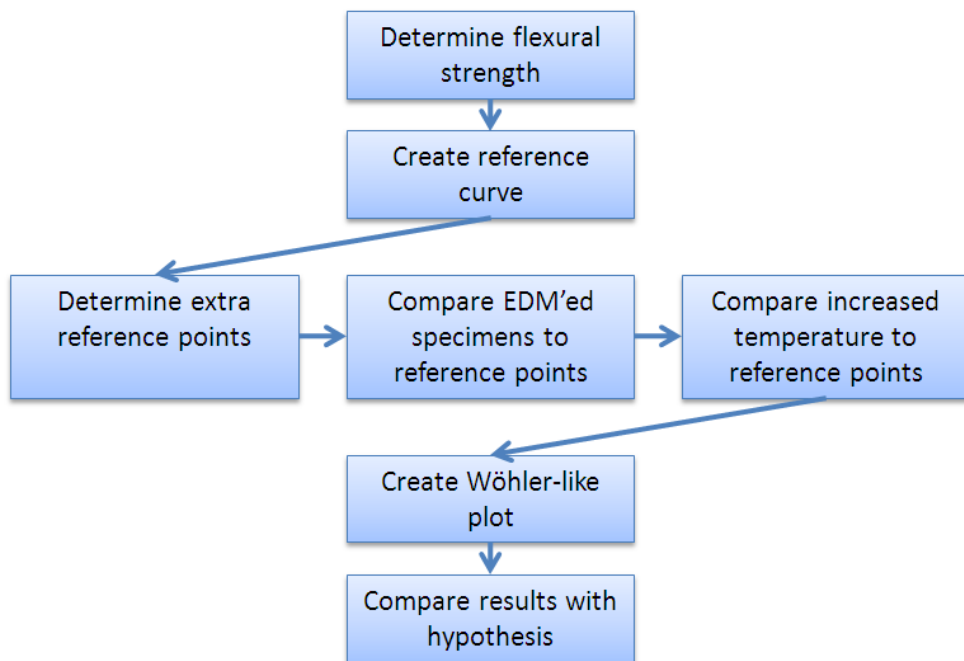


Figure 5-2 Outline of test setup

## 5.2 PRINCIPLE

Mechanical strength of cemented carbides is usually measured by performing a three point bending test (also called three point flexural test or transverse rupture test). The reason for this is that these materials, due to their brittle nature, are very sensitive to misalignment, notches and surface defects. In flexural tests these flaws do not cause problems.

The flexural strength of a material is determined by placing a standard specimen between two supports and loading it until fracture occurs (see Figure 5-3).

The flexural strength is calculated using equation (10) in paragraph 3.5 and given in  $\text{N/mm}^2$  or MPa.

The test should be performed multiple times because of the expected spread due to the surface and subsurface imperfections generating stress concentrations.

It is only possible to compare test results of specimens with equal size. Larger sized specimens generally show lower flexural strength because statistically they have more (sub-)surface flaws. Smaller sized specimens show the opposite.

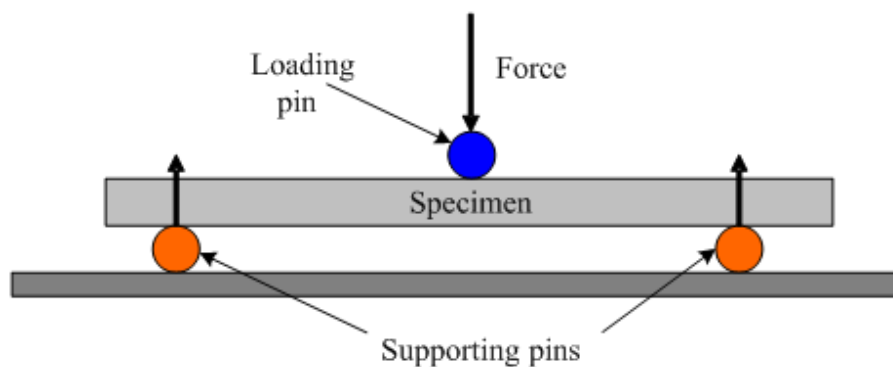


Figure 5-3 Three point flexural test

## 5.3 SPECIMEN

### Material

Literature [15] already indicated that every WC-Co grade shows different fatigue behavior so it is desirable to generate knowledge and testing data on the material used in the process step which causes the most tool fracture. Flattening the running groove of a shaving cap is currently the process step at which the tensile stresses are the highest. The flattening tool is made of the P1030 grade cemented carbide because research at Philips performed in the past shows that this is the most appropriate grade for this process step. Considering the previous this material is also used in the generation of the reference curve.

The P1030 specimen material used for the tests is provided by Ceratizit and there coded as MG18/HIP. See appendix 9 for the Ceratizit test report of the material.

What should be noted is that the Philips datasheets show a transverse rupture strength of 3,0 GPa whilst Ceratizit datasheets suggests that this material shows a transverse rupture strength of 3,7 GPa. An investigation [29] on the

static strength of P1030 and the influence of roughness and machining technique on this static strength is performed slightly in advance of this investigation. This investigation on static strength shows that the value given by Ceratizit is the correct one but is only valid if the specimens are grinded and not annealed afterwards. Ceratizit also confirms that the specimens used for their data are grinded.

#### **Dimensions** (see drawing in appendix 3)

The specimens used for testing are 3 x 9,5 x 50mm. The length of the specimens is chosen 50mm to reduce the force required for fracture to a level which can be reached by the testing apparatus available at Philips. The span of the test setup is only 40mm, but to ensure that the specimen will not slide of it has to be longer than this. Longer specimens where also possible, but would result in an increased price. The reason for this is that the base material is delivered in plates (dimensions 100 x 100 x 3,3mm) and two specimens lengths would not fit in the length or width of the plate anymore.

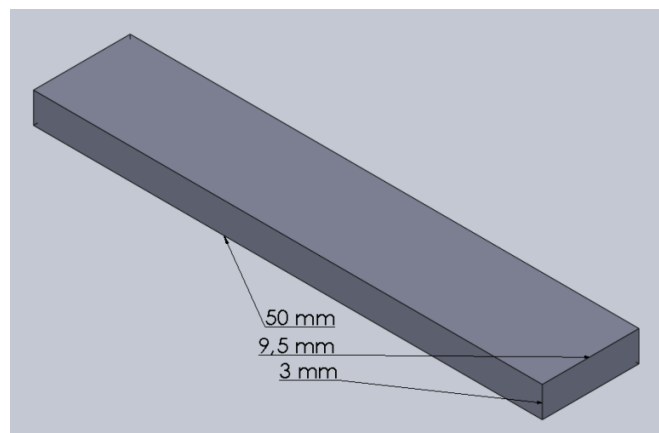


**Figure 5-4 Sample dimensions**

The width of the specimen is chosen 9,5 mm because it would be possible to obtain twenty specimens out of one plate of base material. More width would result in more expensive specimens but also in a higher force required for fracture. This required force is limited by the equipment boundaries (see paragraph 5.4).

The height of the specimen is chosen 3 mm. The reason for this dimension is that fracture will be possible by using the testing apparatus mentioned earlier.

The exact dimensions, tolerances and roughness values of each specimen used for the tests can be found in the appendix (Appendix 4)

#### **Machining technique**

All specimens are supplied by B&S Technology Tilburg. The specimens needed to create the reference curve and the increased temperature test have a grinded tensile side. This side is also prepared by B&S Technology.

The grinding direction is chosen perpendicular to the tensile direction to match the current production process of the cold forming tools as good as possible.

Due to confidentiality reasons B&S Technology does not want to disclose their process settings to create the specimens. This should not be a problem because research performed by Hegeman et al. [24] shows that obtained results are primarily determined by the WC grain size and that differences in grinding parameters have only little effect.

The specimens to verify the EDM effect are supplied by B&S Technology and subsequently grinded (pretreatment) and then EDM'ed on the tensile side by Norma IMS. The grinding process is necessary to generate a flat surface. The EDM process used is sinker EDM (zinkvonken) and is performed in two ways:

- One finishing cut (6 specimens)
- Rough cut, followed by one intermediate cut and one finishing cut (6 specimens)

This last method is comparable to regular tooling production. Due to confidentiality reasons also Norma IMS does not want to disclose their process settings used to create the specimens.

The reason that sinker EDM is chosen is that this type offers the possibility of complex three dimensional shapes.

### Roughness

The roughness of the grinded specimens is chosen  $Ra = 0,03 \mu\text{m}$ . This roughness is also used in the flattening tools in current processes.

The mean roughness obtained using the grinding process is  $Ra = 0,027 \mu\text{m}$ .

The roughness of the EDM'ed specimens was not predefined because of the lack of knowledge about the achievable roughness. The supplier (Norma IMS) was asked to deliver the specimens as smooth as possible with the currently available process.

The obtained roughness of the specimens depends on the process they were subjected to:

- One step EDM'ing resulted in an average roughness of  $Ra = 0,34 \mu\text{m}$
- Three step EDM'ing resulted in an average roughness of  $Ra = 0,29 \mu\text{m}$

### Roughness (an-)isotropy

A complementary roughness measurement performed on an "Alicona InfiniteFocus" showed that the roughness of the specimens is a little anisotropic (directionally dependent). The table below shows the difference in results when measuring parallel and perpendicular to the tensile direction. It also shows the offset between the Alicona and the Mahr measurement when measuring parallel to the tensile direction.

Table 1 Roughness values

Production technique	Ra ( $\mu\text{m}$ ) (parallel to tensile direction) - Alicona	Ra ( $\mu\text{m}$ ) (perpendicular to tensile direction) - Alicona	Ra ( $\mu\text{m}$ ) (parallel to tensile direction) - Mahr
<b>Grinding (specimen B01)</b>	0,032	0,027	0,027
<b>EDM (1 step) (specimen B17)</b>	0,269	0,188	0,269
<b>EDM (3 step) (specimen A08)</b>	0,207	0,153	0,207

The difference in roughness of the EDM'ed specimens can be explained by the fact that the electrodes used to machine these specimens are grinded in a certain direction to generate the desired shape. One is able to see that the roughness parallel to the **grinding** direction (perpendicular to tensile direction) is lower than the roughness perpendicular to the **grinding** direction (parallel to tensile direction).

## Quantity

Consulted literature [15, 24] and ASTM directives [9, 21] state that using two to ten specimens to determine an average value is sufficient. A number of five specimens will be used in the test to determine a certain point.

The generation of the Wöhler-like curve will be performed using 29 specimens. According consulted literature and ASTM directives a minimum of 15 specimens is necessary to generate an indicative curve. Because a more specified curve is desired this number is almost doubled.

## Pictures

The surface of all specimens is analyzed by using optical and scanning electron microscopes. Pictures gathered during this analysis can be found in Appendix 4. (Please note that the samples displayed in Appendix 4 are not etched)

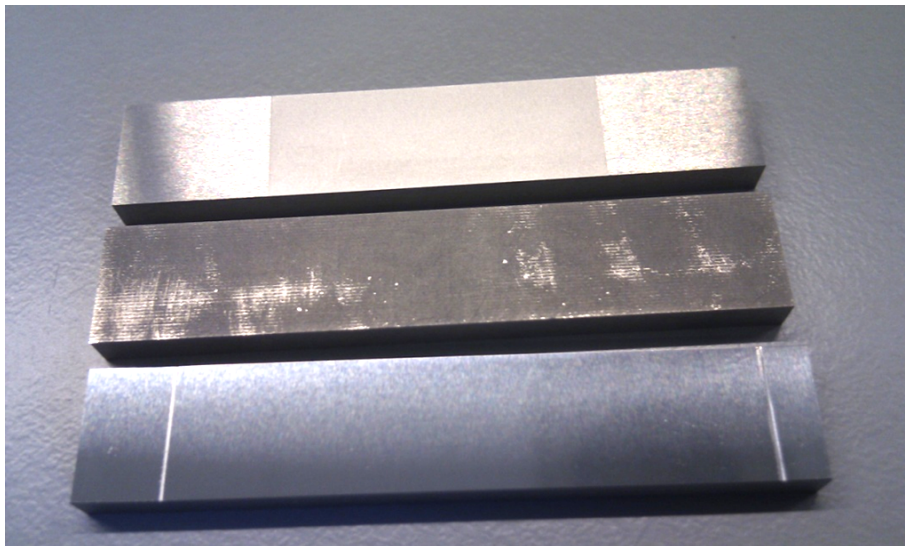


Figure 5-5 Overview of the tensile side of the specimens: EDM, sintered and grinded (from top to bottom)

Figure 4-1 in Appendix 4 shows the pictures taken with the optical microscope. These pictures clearly show the structure of the surface as well as the grinding direction of the grinded specimens. (Note: The tensile stresses during the fatigue tests are oriented left-right)

### *Sintered specimens:*

The left three pictures in Figure 4-2 in Appendix 4 show the sintered surface of the P1030 grade cemented carbide. The tungsten carbides are best visible on the lower most pictures. What also can be seen is that the sintered surface is very uneven and rough, this can also be seen in Figure 5-5.

### *Grinded specimens:*

The right three pictures in Figure 4-2 in Appendix 4 show the grinded surface of the P1030 grade cemented carbide. The lower most picture shows that the tungsten carbides are pulverised and smeared out together with the cobalt binder. A research performed by Hegeman et al. [24] on grinding of WC-Co cemented carbides shows comparable pictures.

The picture taken with a magnification of 1000x shows that some grooves are deeper than others. These grooves are due to damage or impurities on the grinding tools and could be the origin of a fatigue fracture because they act as a stress raiser (notch effect).

*EDM'ed specimens:*

Figure 4-3 in Appendix 4 show the EDM'ed specimens of the P1030 grade cemented carbide. There is a clear visible difference between the left (1 step) and the right (3 step) column confirming the difference in process they experienced.

The lower most pictures show EDM induced cracks. Note that the cracks in the left pictures are larger than the cracks in the right pictures. This can be explained by the fact that crack originating in the EDM process are partly removed when adding a following EDM process (finishing) step.

Adding extra finishing steps is thus better when looking to crack size, but it has to be confirmed by tests if this also counts for the EDM induced stresses.

## 5.4 EQUIPMENT

### Transverse rupture test

The table below lists the equipment used for the flexural fatigue tests:

Part	Manufacturer	Model
Servo hydraulic test rig	Roell/Amsler	STM HC 10 (10 kN)
Digital Controller	Instron	8800
Loadcell	Huppert	1010 BPS 2.5K

(The Instron controller is mentioned separately because it is retrofitted on the Roell/Amsler test rig)

(Datasheets of the used equipment are available on the manufacturer's websites)

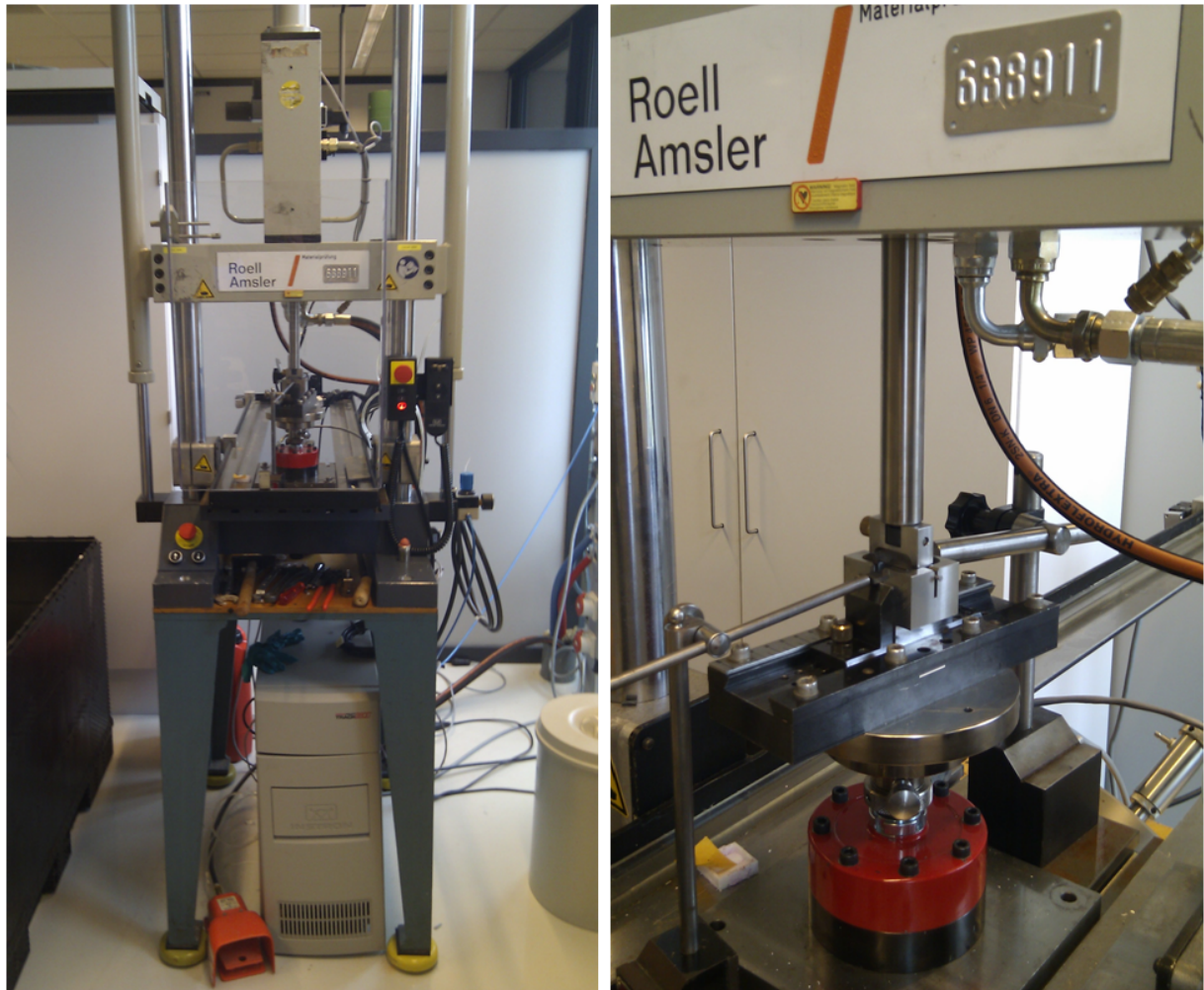


Figure 5-6 Overview of fatigue test equipment

A support designed by Zwick for testing materials on flexural strength and fracture toughness was already present at the test laboratory. Being designed for static failure this support did not provide locking of the specimen to

prevent movement during the fatigue tests. Therefore an extra solution had to be found that prevented movement of the specimen and did not influence the results, a so called position aid. The second goal of the position aid was to prevent the punch of the test rig from rotating during the fatigue tests. A 3D model of the support is shown in Figure 5-7. A drawing of the position aid can be found in appendix 10.

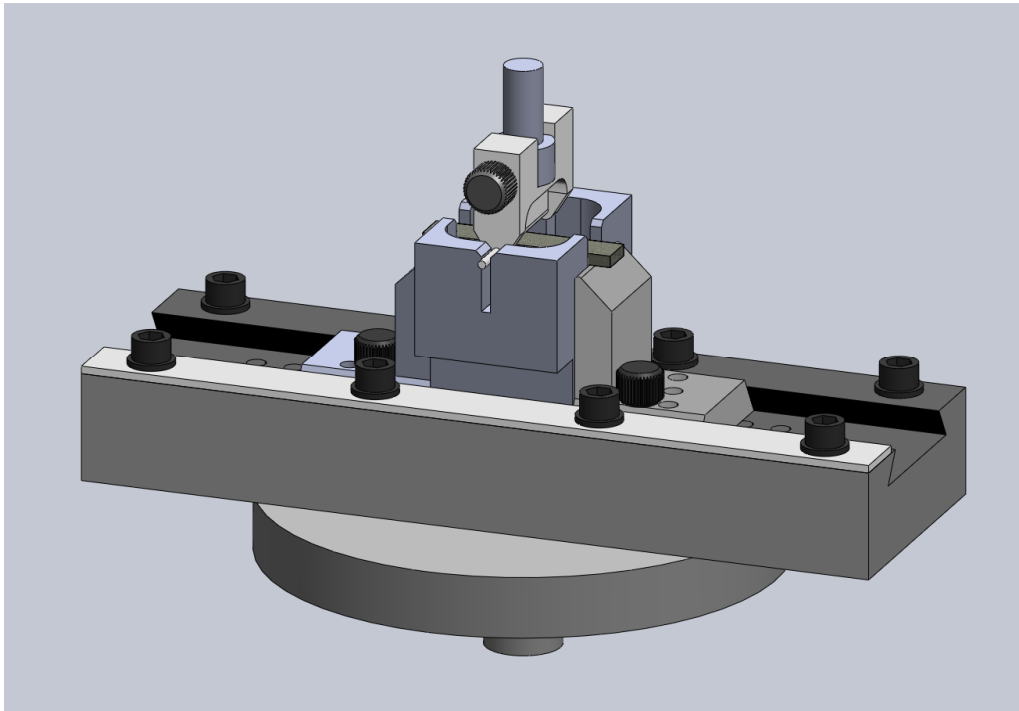


Figure 5-7 Support used for fatigue tests (3D model)

### **Roughness measurement**

The roughness of all specimens is measured by a “Mahr LD 120” measuring unit. (See manufacturers website for datasheet).

The complementary roughness measurement to check the results obtained by the Mahr apparatus is performed on an “Alicona InfiniteFocus” optical microscope. This microscope compares multiple images by means of focus variation.

### **Hardness measurement**

The hardness of all specimens is measured by a LECO V-100-C hardness tester.

## 5.5 PROCESS

### Force determination

By rewriting equation (10) one is able to determine the required force for static failure when the dimensions and the flexural strength are known. The following equation:

$$\sigma = \frac{3FL}{2bd^2} \quad (10)$$

Becomes:

$$F = \frac{2\sigma bd^2}{3L} \quad (21)$$

If the values are:

- $\sigma = 3,7 \text{ GPa} = 3,7 * 10^3 \text{ MPa} = 3,7 * 10^3 \text{ N/mm}^2$
- $b = 9,5 \text{ mm}$
- $d = 3 \text{ mm}$
- $L = 40 \text{ mm}$

A value of 5273 N is obtained for  $F$ . This value is the expected force needed for fracture in a single cycle. Validation of this value is done in another Philips research [29]. Also Ceratizit is contacted to verify their test method. The Philips research and Ceratizit confirm that grinded and/or polished specimens achieve this transverse rupture stress level.

To generate the Wöhler-like curve every next specimen is tested at a 200 N lower force level. After reaching  $10^7$  load cycles, the results are plotted and extra datapoints are indicated at which the other specimens are tested. These points are picked so that the expected number of load cycles will be between  $10^4$  and  $10^6$  because only these values will be interesting.

The force required for cracking the specimen in excess of  $10^7$  cyclic loads is the lowest in this series and is expected to be at around 50% of the required force for static fracture. The remaining specimens are used to redo this exercise at in between values and generate a more detailed and thus more specified curve.

### Stress level for comparison

According to consulted literature cemented carbides show a relative large scatter in fatigue test results. Especially at high cycle numbers the spread is high according to [27, 28]. Because of the finite number of specimens a stress level has been chosen at which  $10^5$  load cycles can be reached for the grinded specimens used to create the reference curve. At this stress level the grinded specimens are compared to the EDM'ed specimens and the specimens tested at increased temperature. This stress level for the reference curve (grinded specimens) is 2280 MPa or 3250 N.

### **Cycle frequency**

Investigations [20] performed in Germany at the 'Universität Erlangen-Nürnberg' show that cemented carbides show a frequency independent fatigue behavior at room temperature. What should be noted is that this is only measured for testing frequencies in the 2-50 Hz range. At high temperatures (700°C and up) or in corrosive environments the fatigue behavior depends on the frequency used for testing (as can be read in paragraph 4.5).

In other consulted literature test frequencies are used varying from 0,5 Hz [8] to 170 Hz [12].

Considering the previous, all fatigue tests in this investigation are performed at 50 Hz. This frequency is chosen relatively high to shorten the required testing period without affecting the fatigue behavior. Still, reaching  $10^7$  cycles requires almost 56 hours.

### **Environmental temperature**

The testing of the specimens used to create the reference curve is performed at a temperature of around 20°C. The EDM'ed specimens are tested at the same temperature level.

The specimens used for the increased temperature test are tested inside a climate chamber at 250°C, the maximum temperature of this component.

### **Hardness**

The hardness of the tensile side of nearly all specimens is measured using a Leco V-100-C hardness tester but since no polishing techniques are used these measurement are only a rough indication of the actual hardness of the specimens. These hardness measurements are performed after the fatigue tests to prevent the indent from a possible role as stress raiser.

The average hardness of the specimens is 1643 HV30 with a standard deviation of 16 HV30. This hardness is in accordance with the specification of the P1030 cemented carbide grade (see Appendix 9).

Please note that the high surface roughness of the EDM'ed specimens did not allow valid hardness measurements but the surface of the grinded specimens was smooth enough to perform hardness measurements.

## Waveform

All specimens are tested using a sinusoidal waveform. The crest (piek) of the waveform will result in the maximum stress in a cycle and will be at a constant level. The trough (dal) of the waveform is at a positive 100N to ensure that the specimen and the punch will always be in contact. This is done to prevent unforeseen effects and excessive noise and it should also help to prevent motion of the specimen due to friction between the specimen and its supports.

As stated in paragraph 4.5 the use of a non-zero trough in the waveform will not have a remarkable effect on the results. The determining parameter is the maximum stress applied. This enables the comparison between the tests and a cold forming process in which the trough is equal to zero.

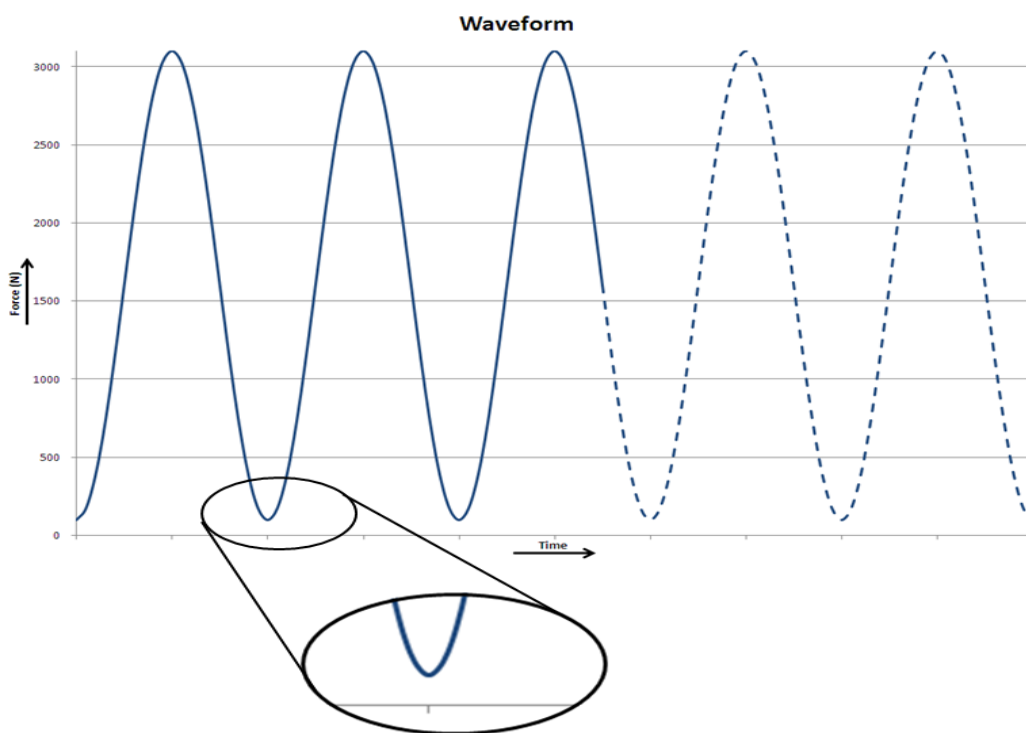


Figure 5-8 Desired waveform with non-zero trough

The correct PID settings of the test equipment were determined by using a damaged grinded specimen. During the tests the waveform is continuously monitored and corrected dynamically if necessary. This method ensures that the crests and troughs of the waveform will return to their predetermined values in every cycle.

## 5.6 RESULTS

### Flexural (static) strength

The Philips research performed by M. v/d Schrootbrugge [29] on static strength of the P1030 grade cemented carbide resulted in the following graph:

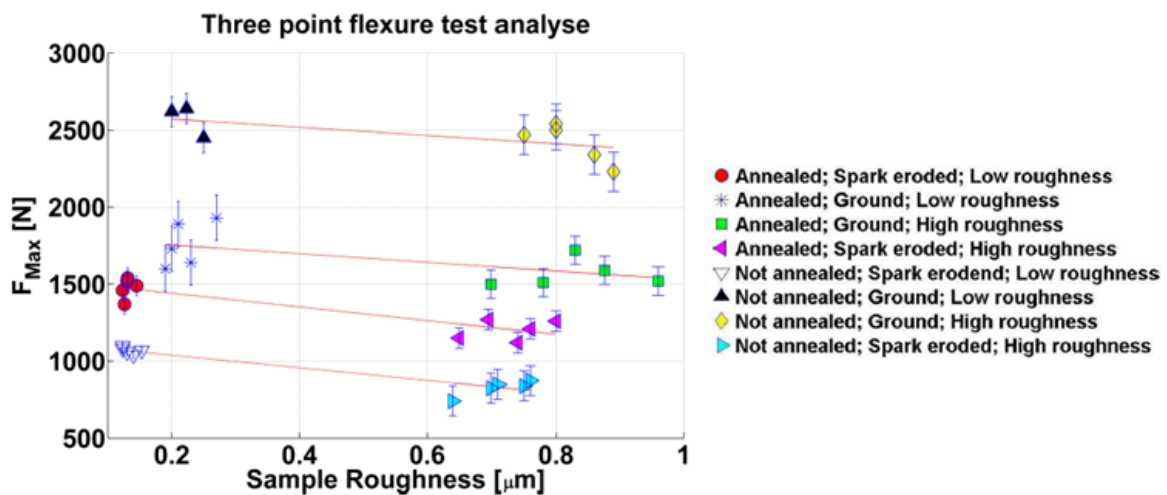


Figure 5-9 Three point flexure test analysis (Force (N) x 1,5 = Stress (MPa)) [29]

The static strength of the grinded specimens with low roughness is equal to the value given by Ceratizit in their datasheet (3,7 GPa).

The offset in strength between the grinded and the EDM'ed specimens is clearly visible in the figure above. The EDM'ed specimens with low roughness show a transverse rupture strength of 1650 MPa. This value is 55% lower compared to the grinded specimens.

Another set of specimens, grinded and EDM'ed, was annealed (8 hr @ 900°C in high vacuum and afterwards slow cooling with max -22°C/hr) to remove the stresses induced by the machining process.

The test results of these annealed specimens show a decreased in offset to only 15%. Another results of this test in [29] is that the induced stresses due to the grinding process are compressive and those generated by the EDM process are tensile.

Figure 5-9 also shows that roughness has an influence on the strength of the specimens. Lower roughness leads to higher strength and vice versa.

Another observation in [29] worth mentioning is that the spread in results is rather high.

### Wöhler-like curve

The attempt to generate a Wöhler-like curve was performed with 35 specimens (30 for the curve, 5 for one extra reference point).

The figure below shows the data points generated during the tests.

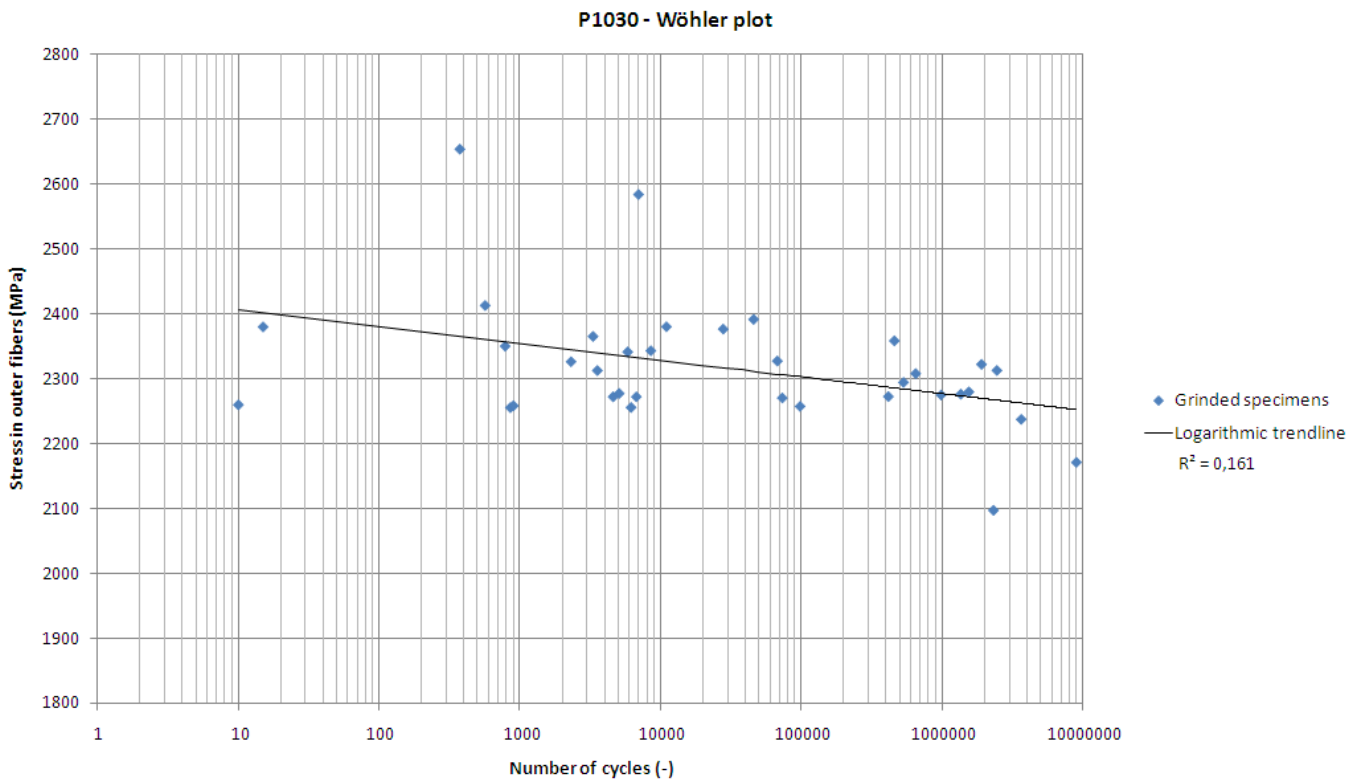


Figure 5-10 Wöhler plot

The logarithmic trendline, obtained by nonlinear regression, in the figure above suggests a linear trend. Unfortunately the  $R^2$  value (coefficient of determination) is very low, meaning that the gathered data points do not correspond very well to this trendline. (A trendline is most reliable when its  $R^2$  value is at or near 1).

The large spread in results is probably due to the grinding direction chosen. As mentioned earlier the specimens are grinded perpendicular to the tensile direction. Closer observation of the edges of the specimens show edge pitting, despite the mirror-like finishing of the surface (see Figure 5-11). The size and shape of these pits are random, and could be responsible for the rather random results. Also grooves due to an imperfection in the grinding tools (see Figure 4-2) could be origins of the large spread.

Despite the large spread in results it seems that the slope of the trendline in Figure 5-10 indicates that this cemented carbide grade does show signs of fatigue behavior. If this was not the case, the trendline would be horizontal.

The small slope of the trendline could be an effect of the large spread, but could also be explained by the material withstanding a high threshold stress intensity ( $K_{th}$ ) or have a high fatigue limit ( $\sigma_f$ ). If this is the case the fatigue sensitivity is very low, meaning that the formulas  $K_{th}/K_{Ic}$  or  $\sigma_f/\sigma_c$  will result in relative high values.

Despite the large spread these results appear to confirm the hypothesis that also the very brittle P1030 cemented carbide grade does show a certain fatigue behavior.

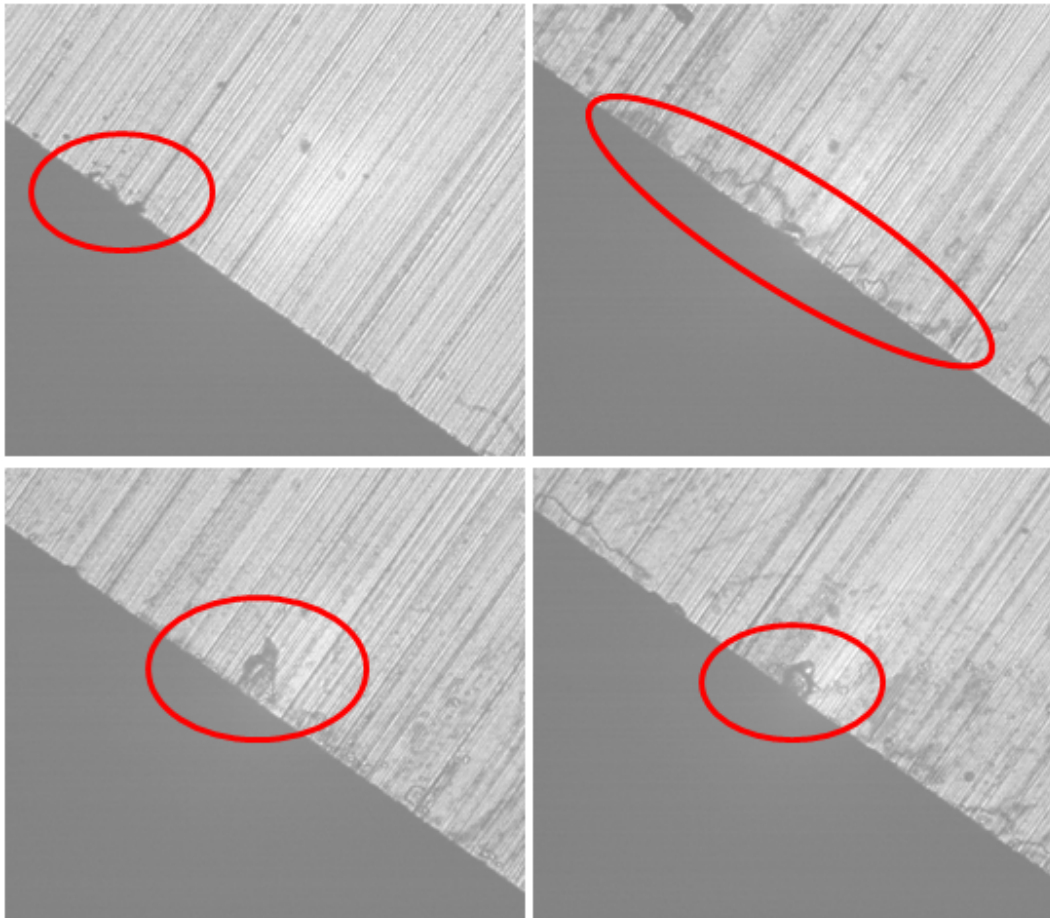


Figure 5-11 Pitting on the edges of the grinded specimens (identical magnification)

### Reference point

After the attempt to create a Wöhler-like curve, five specimens are tested at an equal stress level (2275 MPa). The average number of load cycles these specimens endured is  $5,5 \cdot 10^5$ . Unfortunately the standard deviation is higher than the average making it impossible to determine a valid standard deviation.

### Increased temperature

Despite the large spread in results generated by testing at room temperature another five samples are tested at a temperature of 250°C.

The samples used in this increased temperature test are randomly taken from the stock of grinded samples to try to exclude any possible difference in entry material.

The results of the test can be seen in Figure 5-12. The two left green marked test results are probably due to the earlier mentioned edge damage or a material flaw at the outer fibers. This probably also counts for the three left blue marked results. Unfortunately this cannot be confirmed because of the damage that occurred during the fracture of the specimens.

If only the results around and above the  $10^5$  cycles are considered a remarkable outcome can be seen. All grinded samples lasted between  $10^5$  and  $2 \cdot 10^6$  load cycles. The four specimens tested at increased temperature all had a run out thus lasting more than  $2,5 \cdot 10^5$  load cycles. After reaching this value the test was stopped but if the test was continued these samples could probably endure a lot more load cycles.



These results suggest that the hypothesis that an increase in temperature will result in better fatigue behavior is valid. But more tests should be performed to validate this because the figure below also suggests that the spread increases at higher temperatures.

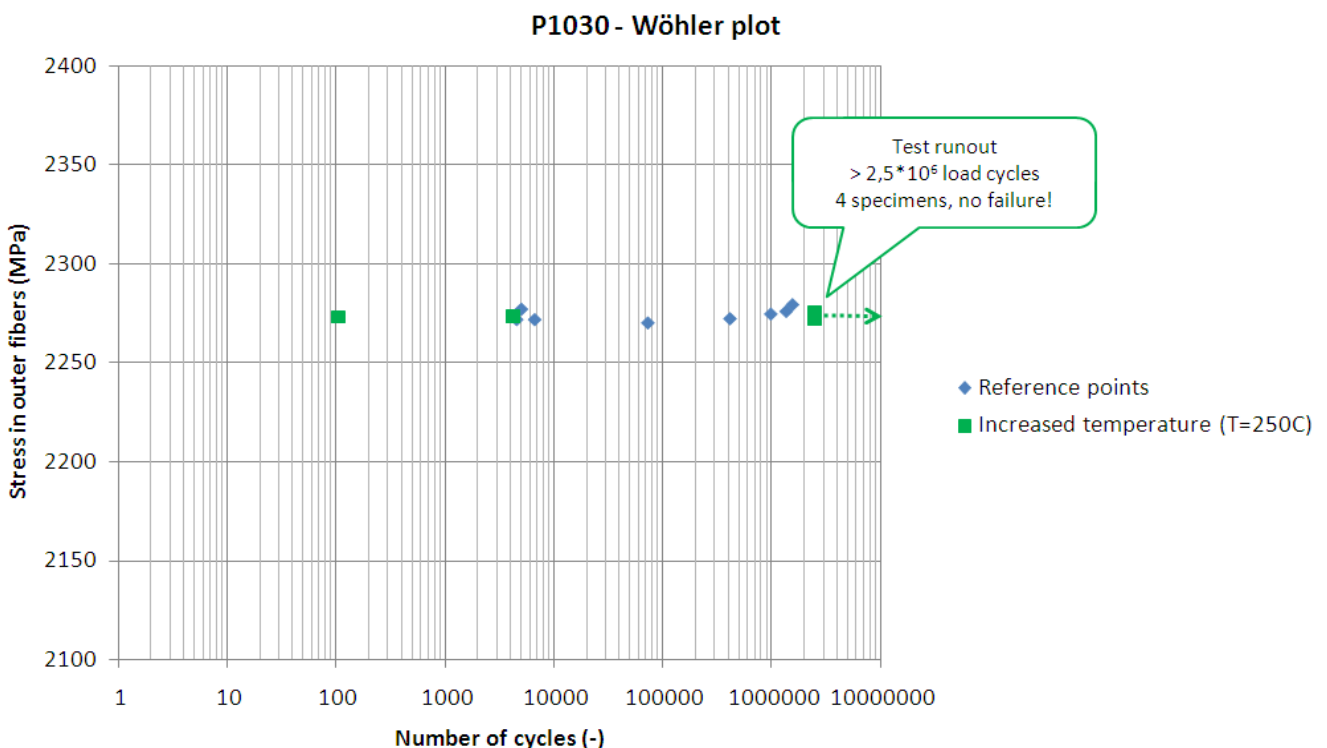


Figure 5-12 Increased temperature test

## EDM effect

As can be seen in Figure 5-13 the EDM'ed specimens show a considerable lower resistance against failure than grinded specimens. The research performed by B. Casas et al. [12] shows comparable results. According to B. Casas and M. v/d Schrootbrugge [29] this is due to the EDM induced tensile stress in the specimens which are added to the applied tensile stress. According to these authors it is possible to remove these induced tensile stresses by a thermal treatment (stress free annealing).

Subsequently, according to Casas and V/d Schrootbrugge, the grinded specimens also show stresses induced by the machining technique but these stresses are compressive(!) and thus result in higher applicable tensile stresses before failure occurs. These stresses can also be removed by a thermal treatment but this is of course not desirable. If annealed grinded and annealed EDM'ed specimens are compared [29], the EDM'ed specimens still show a little lower applicable stress, most probably due to the cracks that originate in the machining process.

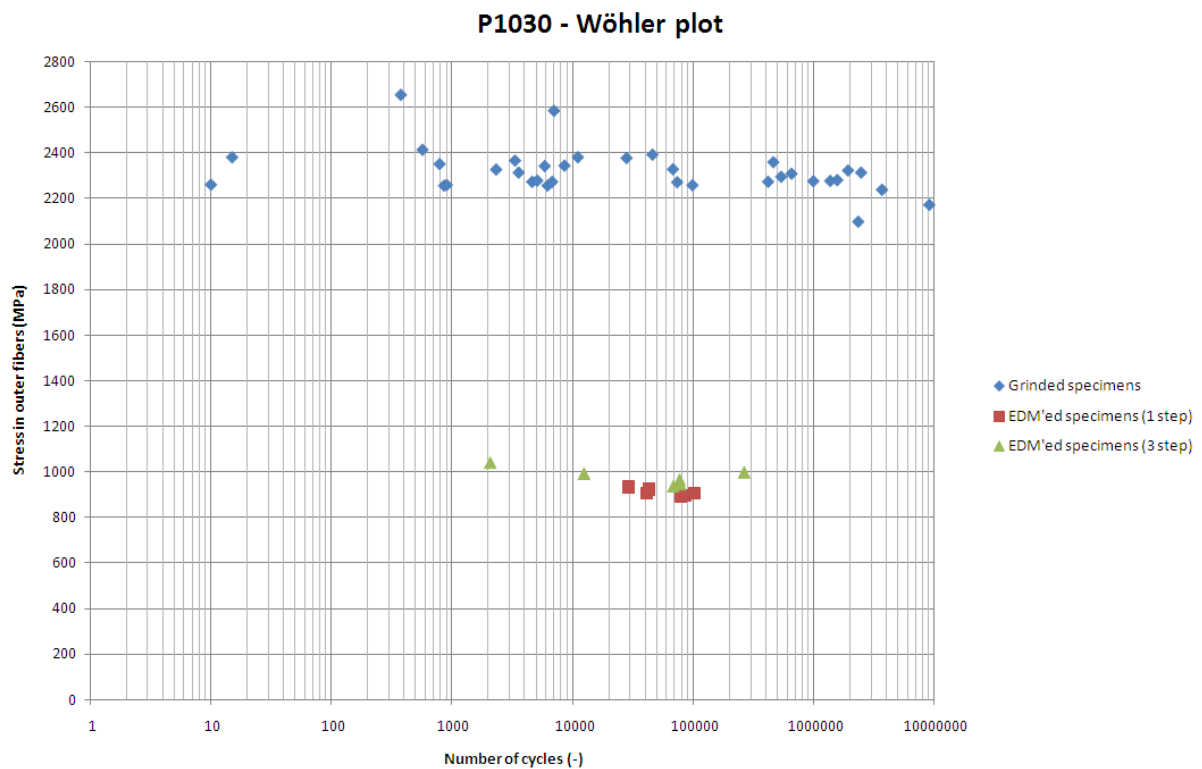


Figure 5-13 EDM versus Grinding

The test results do not allow distinction between the differences in the EDM process. Both specimen sets (1 step EDM and 3 step EDM) seem to have similar results with respect to number of load cycles needed for failure at a given stress level.

These results confirm the hypothesis that EDM'ed specimens do show relative low fatigue strength compared to the grinded specimens. This strength is even that low that testing at the same stress level as the reference specimens were tested was not possible (this was concluded before starting the tests by using the test results of V/d Schrootbrugge [29]).

### Static versus dynamic

The following table shows a comparison between static and dynamic tests. Please note that the fatigue strength for this comparison (third column) is defined as the stress that can be applied to reach  $10^5$  load cycles and **not** as the stress a specimen could endure to survive unlimited (or  $10^7$ ) load cycles.

Table 2 Static versus dynamic

Process	Static strength ( $\sigma_c$ )(GPa)	Fatigue strength ( $\sigma_f$ ) (GPa)	Static / Dynamic ( $\sigma_f/\sigma_c$ ) (-)
Grinded	3,7	2,2	$2,2 / 3,7 \approx 0,6$
EDM'ed	1,4	0,9	$0,9 / 1,4 \approx 0,6$

Please note that the right column in the above table is not the fatigue sensitivity. This could not be calculated because the EDM'ed specimens where tested to break between  $10^5$  and  $10^6$  load cycles and not infinity.

When analyzing Table 2 it is surprising that the fourth column shows identical values. This suggests that a static test is sufficient to differentiate between different machining techniques. But it should be mentioned that only two data points are given in this table suggesting a linear trend and that the ratio in the third column does not have to be valid for the whole range of stress levels and/or machining methods.

### Fracture analysis

All tested specimens show a fracture similar to those displayed in Figure 5-14. The main difference between the fractured specimens is that the grinded specimens shattered into more pieces that the EDM'ed ones. This difference is due to the fact that more energy (force) is required for fracture for grinded specimens in comparison to the EDM'ed specimens.

The main resemblance is that the cracks seem to originate at the edges of the specimens. The most rational explanation of this phenomenon is that the stress at these edges is higher than in the center of the tensile side and pitting is present at these edges. This higher stress combined with the pitting (Figure 5-11) results in an enforced notch effect at the edges of the specimens.

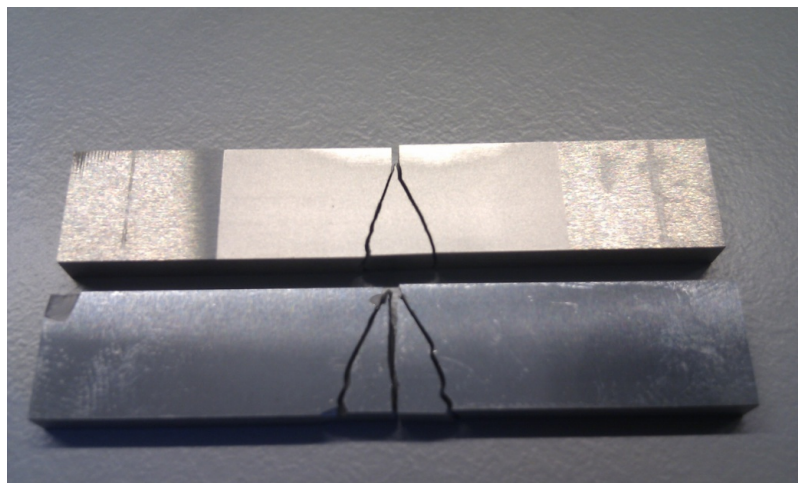


Figure 5-14 Fracture analysis

As expected; fracture analysis did not result in the discovery of beachmarks or striations.

## 6. CONCLUSION

- The P1030 grade cemented tungsten carbide does show signs of fatigue behavior. Applying a certain stress level will result in failure at a number of load cycles. This means that if a specimen survives a low number of load cycles ( $<10^4$ ) it still can fail in the load cycles to come and probably won't be able to endure unlimited load cycles as sometimes is said about brittle materials.
- Grinding in a direction perpendicular to the tensile direction probably leads to high spread in obtained test results. This high spread makes it impossible to use the Wöhler like plot in paragraph 5.6 as a design guideline.
- Despite a finishing method resulting in a mirror-like surface, this method is not good enough to reduce the spread in obtained test results. Microscopic flaws at the edge of the specimens are still present.
- The test performed at increased temperature (250°C) suggests that an increase in temperature is beneficial to the fatigue sensitivity, but also the spread seems to increase.
- The EDM process leads to less spread in test results. Therefore making the fatigue behavior better predictable than the grinded specimens.
- The flexural and fatigue strength of the P1030 grade cemented tungsten carbide is strongly affected by the EDM process. A large offset between the strength of the grinded specimens and the strength of the EDM'ed specimens is present.
- With the test settings used, a static test seems to be sufficient to differentiate between the grinding and EDM finishing methods. Note that this still has to be confirmed for more data points because only two points were investigated.
- Differentiating between one step EDM and three steps EDM with respect to fatigue sensitivity is not possible with the tests performed.
- Macroscopic fracture analysis indicates that cracks originate at the edge of a specimen. This is independent of the applied finishing method suggesting that the stress at the edge is higher than in the center of the tensile side. The cracks initiate at a position vertical of the point where the force is applied.
- A correlation between hardness and fatigue strength cannot be found.



## 7. RECOMMENDATIONS & FUTURE WORK

- The large spread in test results suggests that a probabilistic approach (i.e. Weibull, Birnbaum-Saunders) is better suitable for describing the fatigue behavior of the P1030 cemented carbide grade than a Wöhler curve. Applying Weibull statistics to the current dataset is not possible because more results are necessary (Weibull statistics is based on an infinite number of data points).
- To generate a Wöhler-like curve with less spread the finishing method should be optimized. This can probably be done by grinding in a direction parallel to the tensile direction. Also thorough polishing of the specimens could reduce the spread. Another countermeasure could be a small radius at the edges of the specimens.
- To be able to support the conclusion that a static test is sufficient to predict the fatigue behavior this has to be investigated for more stress levels and other finishing techniques.
- The Wöhler-like presented in Figure 5-10 suggests that below 2000 MPa no fracture occurs. This still has to be validated by tests.
- To verify, quantify and optimize the effect of increased temperature on the fatigue sensitivity another set of test could be performed at different temperatures.
- To reduce the effect that the EDM finishing process has on the specimen's strength the EDM'ed specimens could be annealed. Static tests confirm that this results into increased strength but this still has to be confirmed for dynamic tests.
- The EDM'ed specimens are all finished by the 'sinker EDM' method. It could be very interesting to compare these results with other EDM methods like wire-EDM and micro-EDM.
- Also a comparison with ECM (electro chemical machining) finished specimens would be very interesting because recent research at Philips shows that it is possible to ECM cemented carbides.
- Tests at increased temperature show improvement in durability at a certain stress level and a certain finishing method. It has to be confirmed that this is also valid for multiple stress levels and finishing methods (i.e. EDM).
- Tests at increased temperature sometimes show improvement in durability at a certain temperature level. This temperature level (250°C) is chosen because it is close to the level found in literature (see paragraph 4.5) and it is the maximum level achievable by the climate chamber at Philips. Finding an optimal temperature level with respect to durability is still to be done.



## BIBLIOGRAPHY

- [1] A. v/d Grijn, Philips report: Hardmetaal *Philips Consumer Lifestyle (2005)* 1-10
- [2] K. Brookes, Carbide experts hammer out toughness problems *Elsevier Technical Trends (2004)* 22-25
- [3] <http://www.allaboutcementedcarbide.com> *Sandvik Hard Materials (visited October 2010)*
- [4] A. van Beek, Advanced Engineering Design: Lifetime Performance and Reliability (*Edition 2009*) ISBN 9789081040617
- [5] T.R. Shearer, The designer's guide to Tungsten Carbide *General Carbide (2007)*
- [6] W.D. Callister, Materials Science and Engineering: An introduction *John Wiley and Sons (Sixth Edition, 2003)* ISBN 0471224715
- [7] H. Wildschut, Breukmechanica en vermoeiing *PT Opleidingen, Cursus I&K (1998)*
- [8] Y. Torres, M. Anglada, L. Llanes, Fatigue mechanics of WC-Co cemented carbides *International Journal of Refractory Metals & Hard Materials 19 (2001)* 341-348
- [9] ASTM C 1421 – 01b, Standard Test Methods for Determination of Fracture Toughness of Advanced Ceramics at Ambient Temperature *ASTM International (Reapproved 2007)*
- [10] [http://en.wikipedia.org/wiki/fatigue\\_\(material\)](http://en.wikipedia.org/wiki/fatigue_(material)) *Wikipedia (visited September 2010)*
- [11] M. Kooijman, M. Pallada, Materiaalkeuze voor Ontwerpers *Academic Service (First edition, 2006)* ISBN 9039524653
- [12] B. Casas, Y. Torres, L. Llanes, Fracture and fatigue behavior of electrical-discharge machined cemented carbides *International Journal of Refractory Metals & Hard Materials 24 (2006)* 162-167
- [13] G.S. Upadhyaya, Cemented Tungsten Carbides: Production, properties and testing *Noyes Publications (1998)* ISBN 0815514174
- [14] P.C. Paris, M.P. Gomez, W.E. Anderson, A Rational Analytic Theory of Fatigue *The Trend in Engineering (1961)*
- [15] L. Llanes, Y. Torres, M. Anglada, On the fatigue crack growth behavior of WC-Co cemented carbides *Acta Materialia 50 (2002)* 2381-2393
- [16] Y. Torres, V.K. Sarin, M. Anglada, L. Llanes, Loading mode effects on the fracture toughness and fatigue crack growth resistance of WC-Co cemented carbides *Scripta Materialia 52 (2006)* 1087-1091
- [17] J.A.M. Ferreira, M.A. Pina Amaral, F.V. Antunes, J.D.M. Costa, A study on the mechanical behavior of WC-Co hardmetals *International Journal of Refractory Metals & Hard Materials 27 (2009)* 1-8
- [18] H. Klaasen, J. Kübarsepp, F. Sergejev, R. Traksmaa, Performance of cemented carbides in cyclic loading conditions *Material Science (Medžiagotyra) 12 (2006)* 144-146

- [19] P. Kindermann, P. Schlund, H.-G. Sockel, M. Herr, W. Heinrich, K. Görting, U. Schleinkofer, High-temperature fatigue of cemented carbides under cyclic loads *International Journal of Refractory Metals & Materials* 17 (1999) 55-68
- [20] V.A. Pugsley, H.-G. Sockel, Corrosion fatigue of cemented carbide cutting tool materials *Materials Science & Engineering A366* (2004) 87-95
- [21] ASTM E 647 – 08, Standard Test Method for Measurement of Fatigue Crack Growth Rates *ASTM International* (Approved 2008)
- [22] B. Roebuck, C.J. Maderud, R. Morrell, Elevated temperature fatigue testing of hardmetals using notched testpieces *International Journal of Refractory Metals & Materials* 26 (2008) 19-27
- [23] B. Lauwers, J.-P. Kruth, W. Eeraerts, Wear behavior and tool life of wire-EDM-ed and ground carbide punches *CIRP Annals – Manufacturing Technology* 54 (2005) 163-166
- [24] J.B.J.W. Hegeman, J.Th.M. De Hosson, G. de With, Grinding of WC-Co hardmetals *Wear* 248 (2001) 187-196
- [25] N.V. Novikov, V.I. Kushch, S.I. Shestakov, Stress, strength and durability analysis of gradient-structured hardmetal products *Strength of Materials* 39 (2007) 116-127
- [26] F. Sergejev, I. Preis, I. Hussainova, J. Kübarsepp, Fatigue mechanics of TiC-based cemented carbides *Proceedings of the Institution of Mechanical Engineers Part J: Journal of Engineering Tribology* 222 (2008) 201-209
- [27] H. Klaasen, J. Kübarsepp, I. Preis, Wear behaviour, durability, and cyclic strength of TiC base cermets *Material Science and Technology* 20 (2004) 1006-1010
- [28] ASTM C 1161 – 02c, Standard Test Method for Flexural Strength of Advanced Ceramics at Ambient Temperature *ASTM International* (Reapproved 2008)
- [29] M. v/d Schrootbrugge, On the fracture mechanics and fracture morphology of P1030 tungsten carbides *Internal Philips report* (2010)





## 1. MECHANICAL PROPERTIES

Material selection is based on material properties. Material properties are quantitative properties that enable the comparison of materials. These properties are intensive, meaning that it is a physical property of a system that does not depend on the size or the amount of material in the system.



Material properties can be constant or a function of one or more independent variables. What should be noted is that material properties can vary slightly with the degree in which they are measured. This is called anisotropy.

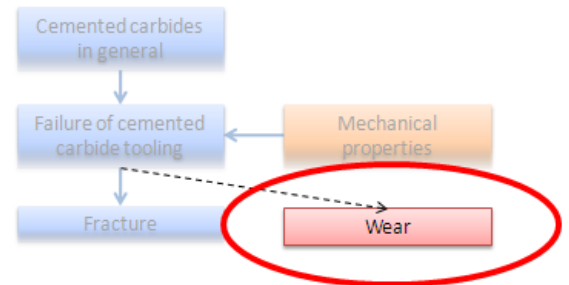
For cold forming the mechanical properties are of most interest. These properties describe the different types of external forces and stresses that a material can withstand. Also the specific weight of a material is a mechanical property. To help understanding the main text of this thesis some mechanical properties are listed in Table 3 for convenience:

Table 3 Key mechanical properties in alphabetical order [6]

<b>Compressive strength</b>	The ability of a material to withstand compressive loads without being crushed
<b>Ductility</b>	A measure of a material's ability to undergo plastic deformation before fracture
<b>Fatigue limit</b>	The stress level below which a material never fails regardless of the number of cycles
<b>Flexural modulus</b>	Comparable to the Young's modulus in three point bending tests (see Young's modulus)
<b>Flexural strength</b>	(Transverse rupture strength) The stress at the outer fibers in a flexural test (buigproof)
<b>Fracture toughness</b>	The resistance to fracture when a crack is present
<b>Hardness</b>	The resistance of a material to deformation by surface indentation
<b>Poisson's ratio</b>	The negative ratio of lateral and axial strains that results from an applied axial stress
<b>Shear modulus</b>	The ratio of shear stress to shear strain when deformation is totally elastic
<b>Shear strength</b>	The maximum engineering stress, in shear, that may be sustained without fracture
<b>Specific modulus</b>	The ratio of elastic modulus to specific gravity for a material
<b>Specific weight</b>	The weight per unit volume of a material
<b>Tensile strength</b>	The maximum engineering stress, in tension, that may be sustained without fracture
<b>Toughness</b>	A measure of the amount of energy absorbed by a material as it fractures
<b>Yield strength</b>	The stress required to produce a very slight, specific amount of plastic strain
<b>Young's modulus</b>	The ratio of stress to strain when deformation is totally elastic

## 2. WEAR

The usability of cemented carbide tooling is limited by either wear or fracture. Wear is the gradual degradation of the tooling; the tooling is still intact, but the dimensions are changing slowly (sometimes it is possible to correct the changed tooling by post processing them until the desired specifications are met again). Fracture is the (sudden) separation of the tooling into two or more pieces; this makes it impossible to continue with the production process.



Cemented carbides are primarily used in cold forming processes because of their excellent wear resistance. Accurately spoken, wear isn't a material property but a system property. This means that not only the material itself, but also its roughness, lubrication, loading and environment are determining the wear behavior.

### Wear in cold forming

Because of the many possible origins of wear it is important to analyze and/or predict the wear behavior carefully to be able to choose a correct grade of cemented carbides for tooling.

In the cold forming processes four different wear mechanisms are dominant: adhesive wear, abrasive wear, corrosive wear and surface fatigue. These wear mechanisms take place at the interface of two contacting bodies and are therefore classified as two-body wear mechanisms.

### 2.1 ADHESIVE WEAR

Adhesive wear occurs if two contacting bodies, moving relative to each other, exhibit high metallurgical compatibility and start to show micro welding. This means that materials sheers off and starts to transfer to the other body. This transfer can be temporary, resulting in free wear particles, or permanent, and thus changing the shape of the tooling.

Lubrication can minimize adhesive wear by preventing surface contact between the two bodies.

Specific forms of adhesive wear are: scuffing, scoring, cold welding and galling.



Figure 2-1 Example of adhesive wear [4]

## 2.2 ABRASIVE WEAR

Abrasive wear occurs in two modes; two-body and three-body abrasive wear. In two-body abrasive wear constrained asperities of the harder material plough into the surface of the softer material (comparable with sanding using sandpaper). Three-body adhesive wear refers to non constrained hard particles in between two contacting bodies ploughing at least one of the two surfaces.

Abrasive wear can be minimized by multiple options [4]:

- Difference in hardness between surfaces < 10% (probability of adhesive wear)
- High hardness of both surfaces
- Low roughness of the harder surface
- Embedding of hard particles in softer surface
- Removing hard particles or keeping them away



Figure 2-2 Punch edge showing abrasive wear [4]

## 2.3 CORROSIVE WEAR

Most metals react with oxygen in air or water and start to form an oxide layer. On carbon steels this oxide layer is porous and thus allowing oxygen to access the base material resulting in a continued oxidation process. Stainless steels contain a high amount of corrosion resistant elements: chromium, molybdenum, nickel etc. For these elements corrosion is thermodynamically unfavorable, enabling the formation of a non porous, well adhered layer protecting the base material from further oxidation.

The risk of an oxide layer is that it is susceptible (gevoelig) to high forces and vibrations which can penetrate this layer. A penetrated layer can adhere and abrade away when there is relative movement between the two bodies.



Figure 2-3 Corrosive wear on chrome steel bushing [4]

Cemented carbide particles themselves are resistant to most corrosive media, but the binder material is susceptible to leaching [5]. The binder material will leach from the surface when it is in the presence of a strong acid or alkali, leaving the carbide particles unsupported. These will start to abrade away exposing new surface to the acid or alkali.

Counter measures to minimize corrosive wear are mostly aimed at protecting the material from the corrosive environment by using lubricants and/or coatings. Also lowering the environment temperature will slow down corrosion.

## 2.4 SURFACE FATIGUE

The previously mentioned wear mechanisms mainly occur between sliding surfaces. Surface fatigue generally occurs in cyclic, rolling, loading conditions (e.g. bearings). This cyclic loading generates subsurface crack growth resulting in the delamination of the material's surface.

This damage only occurs after a large number of loading cycles. Until the material starts delaminating it is still functional.

Surface fatigue life expectancy can be increased by [4]:

- Lowering contact pressure
- High hardness
- Low roughness
- Shotpeening

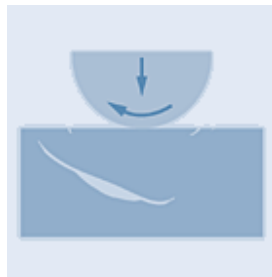


Figure 2-4 Surface fatigue due to rolling contact



#### 4. SAMPLE PICTURES

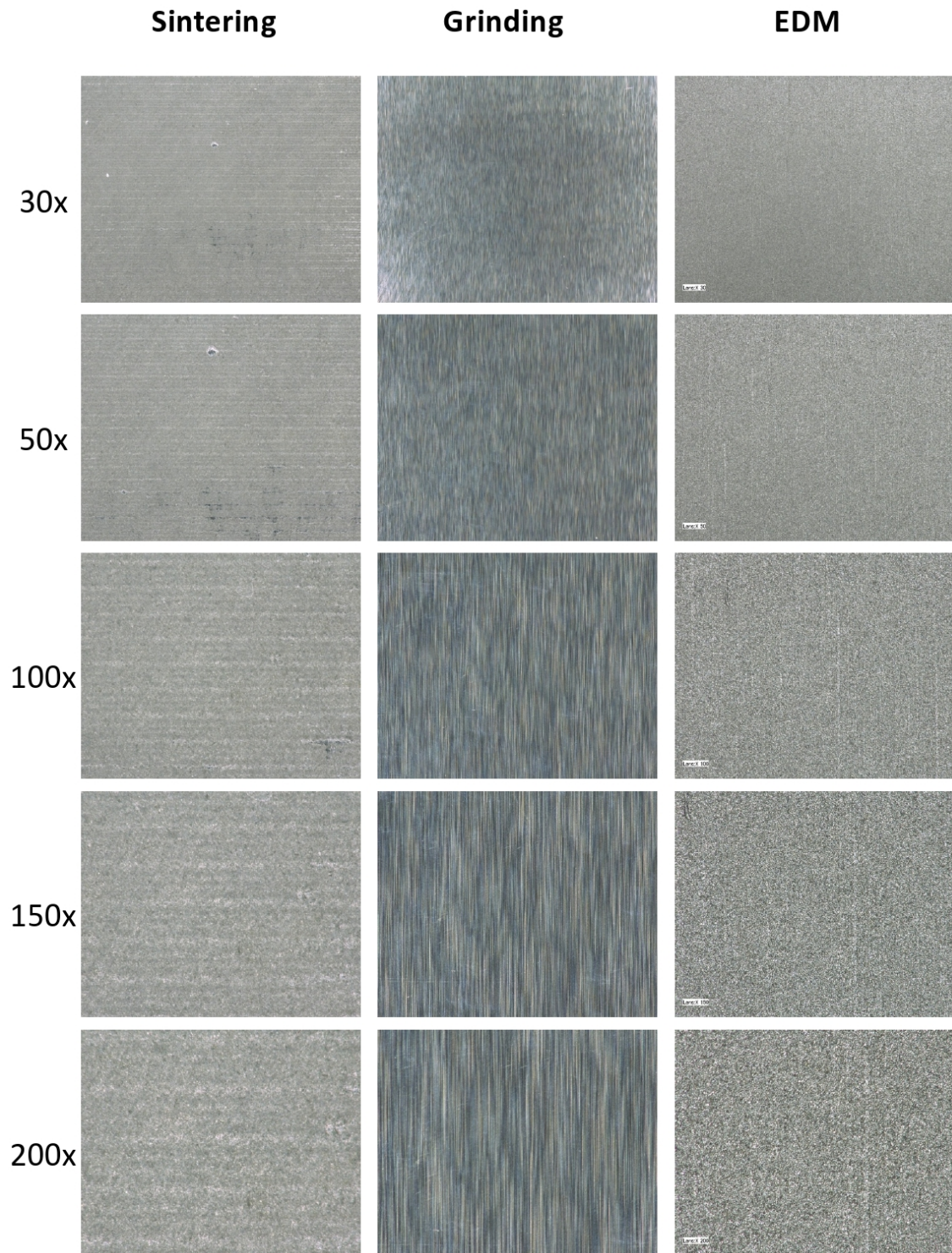
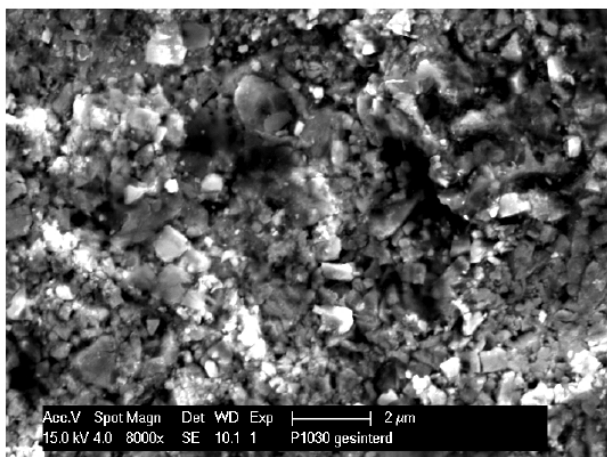
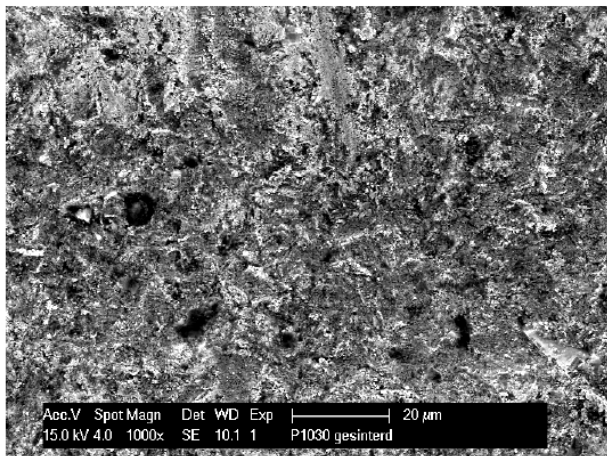
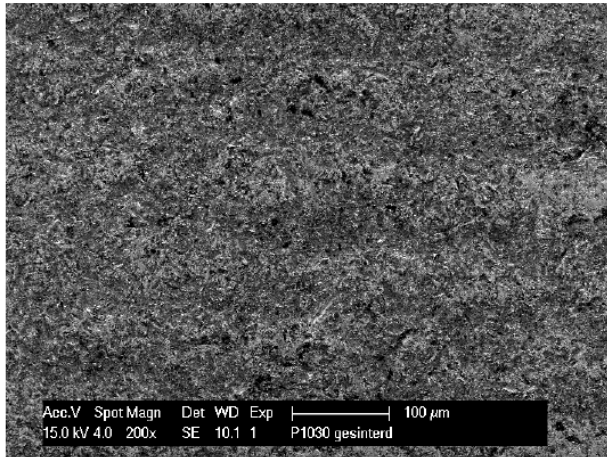


Figure 4-1 Confocal microscope pictures of specimens with different production techniques

## Sintering



## Grinding

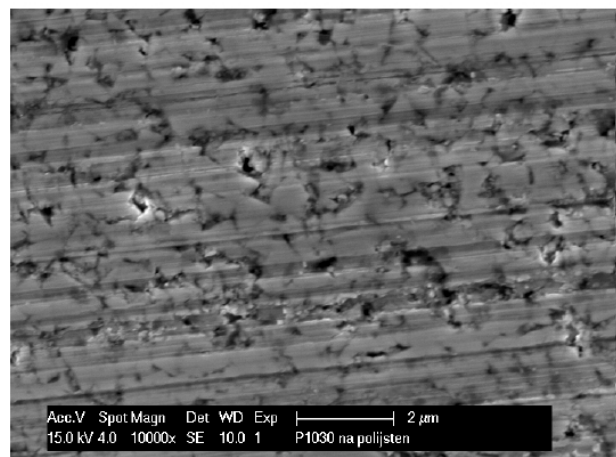
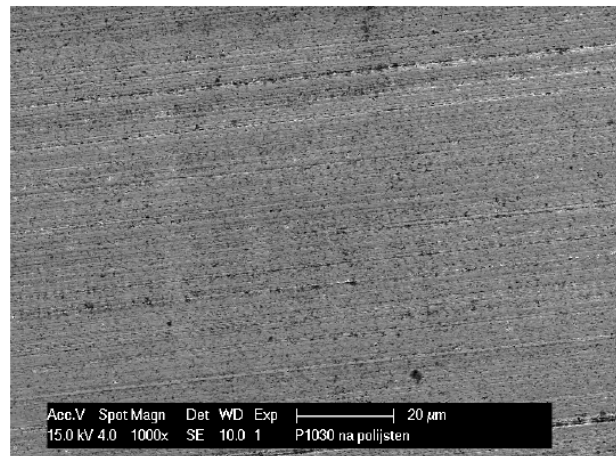
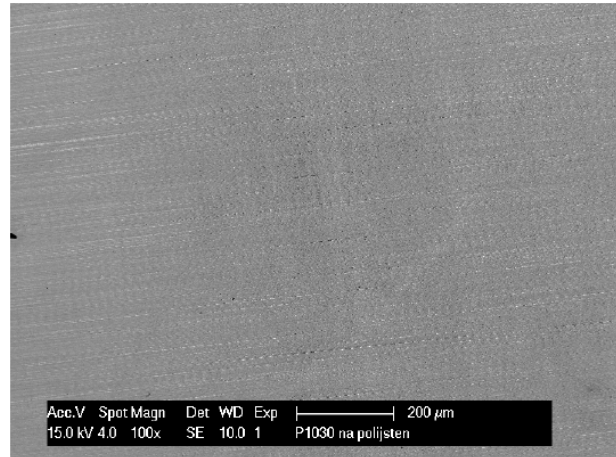
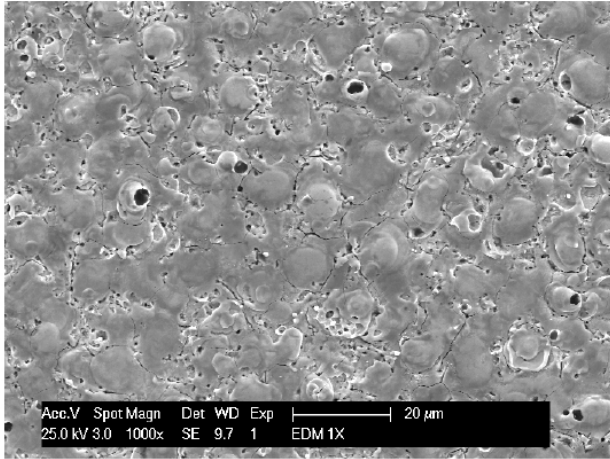


Figure 4-2 SEM pictures of sintered and grinded specimens

### EDM 1step



### EDM 3step

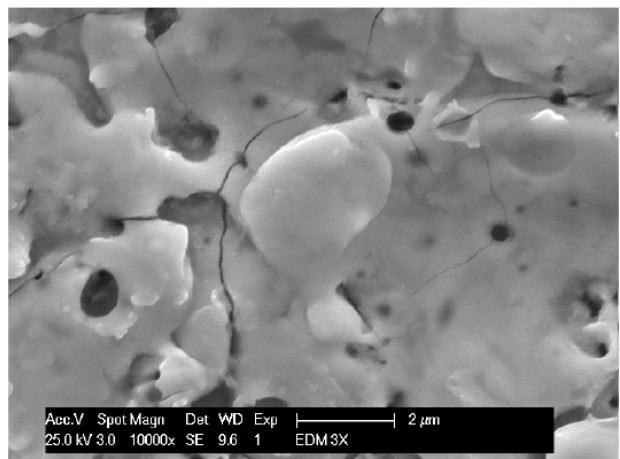
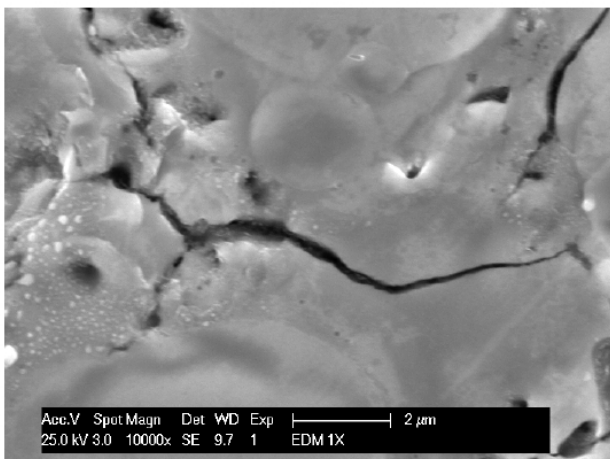
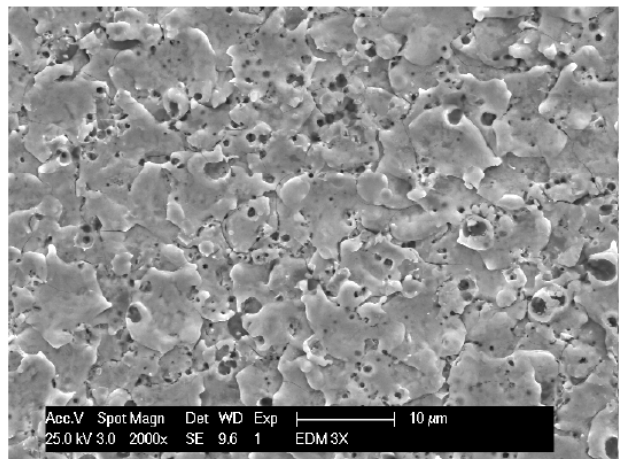
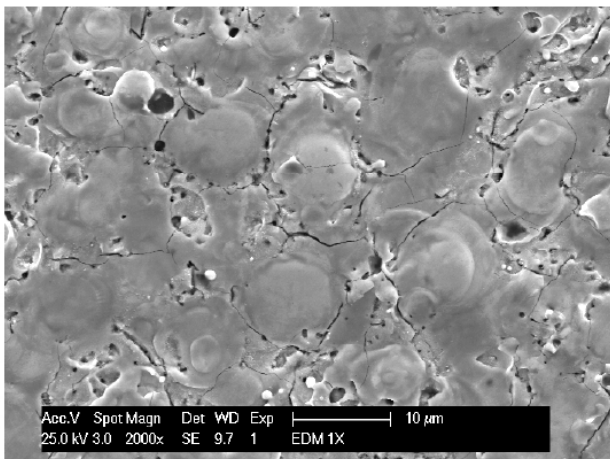
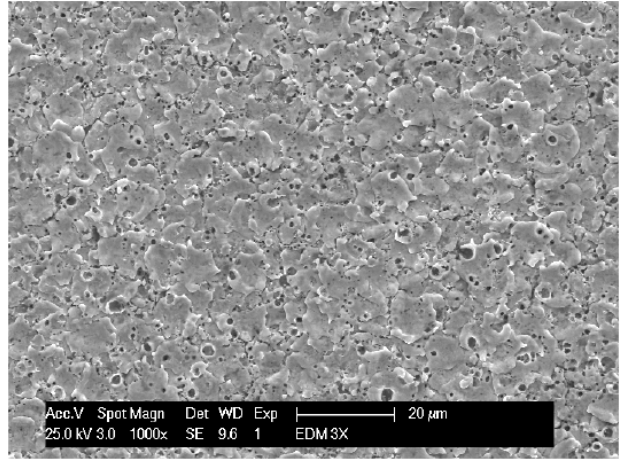


Figure 4-3 SEM pictures of EDM'ed specimens

x | Fatigue behavior of the P1030 cemented carbide grade

## 5. SPECIMEN DATA / TEST RESULTS

Batch	Nr.	Preparation	Test type	Thickness	Width	Applied force	Stress in outer fibers	No. of cycles untill failure	Hardness	Roughness (Ra)
				(mm)	(mm)	(N)	(MPa)	(-)	(HV30)	( $\mu\text{m}$ )
A	1	Grinding	Ref.	3,002	9,284	3700	2653	375	1630	0,034
A	2	Grinding	Ref.	3,004	9,512	3000	2097	2316576	1645	0,034
A	3	Grinding	Ref.	3,002	9,514	3400	2380	15	1616	0,032
A	4	Grinding	T=250	3,003	9,509	3250	2274	4202	1638	0,03
A	5	Grinding	Ref.	3,000	9,513	3300	2313	3550	1659	0,025
A	6	Grinding	Ref. point	3,004	9,509	3225	2255	856	1638	0,023
A	7	Grinding	Ref.	3,002	9,498	3375	2365	3312	1645	0,023
A	8	EDM	3 step	3,102	9,353	1500	1000	264556		0,328
A	9	EDM	3 step	3,113	9,500	1600	1043	2094		0,409
A	10	Sinter		3,126	9,500					
A	11	Grinding	Ref.	3,002	9,513	3400	2380	10998	1667	0,035
A	12	Grinding	Ref.	3,004	9,511	3350	2341	5839	1638	0,025
A	13	Grinding	Ref.	3,003	9,510	3325	2326	2310	1652	0,026
A	14	Grinding	Ref. point	3,003	9,512	3225	2256	6161	1630	0,027
A	15	Grinding	Ref.	3,003	9,513	3300	2308	648691	1645	0,026
A	16	Grinding	T=250	3,003	9,514	3250	2273	106	1645	0,024
A	17	EDM	1 step	3,148	9,498	1450	924	42875		0,336
A	18	EDM	1 step	3,153	9,377	1450	933	29290		0,354
A	19	Sinter		3,154	9,500					
A	20	Sinter		3,120	9,498					
B	1	Grinding	Ref.	3,001	9,512	3100	2171	8987923	1638	0,027
B	2	Grinding	Ref.	3,002	9,510	3325	2327	67505	1630	0,026
B	3	Grinding	Ref.	3,005	9,512	3325	2322	1906217	1652	0,034
B	4	Grinding	Ref.	3,004	9,513	3400	2376	27827	1674	0,024
B	5	Grinding	Ref.	3,001	9,514	3225	2258	900	1645	0,03
B	6	Grinding	Ref. point	3,002	9,511	3250	2275	983051	1630	0,029
B	7	Grinding	Ref.	3,001	9,500	3250	2280	1550000	1630	0,027
B	8	EDM	3 step	3,138	9,501	1550	994	12490		0,245
B	9	EDM	3 step	3,129	9,499	1500	967	77186		0,233
B	10	Sinter		3,201	9,497					
B	11	Grinding	Ref.	3,001	9,512	3275	2294	531751	1645	0,024
B	12	Grinding	Ref.	3,003	9,512	3450	2413	567	1630	0,026
B	13	Grinding	Ref.	3,005	9,514	3425	2391	45732	1682	0,026
B	14	Grinding	Ref.	3,003	9,513	3250	2273	414892	1645	0,025
B	15	Grinding	Ref.	3,004	9,513	3375	2358	458178	1624	0,027
B	16	Grinding	T=250	3,004	9,512	3250	2272	2500000	0	0,025
B	17	EDM	1 step	3,153	9,500	1425	905	102851		0,322
B	18	EDM	1 step	3,154	9,496	1425	905	41520		0,346
B	19	Sinter		3,219	9,497					
B	20	Sinter		3,199	9,499					
C	1	Grinding	Ref.	3,000	9,514	3225	2260	10	1652	0,022
C	2	Grinding	Ref.	3,003	9,513	3350	2343	8516	1645	0,022
C	3	Grinding	Ref.	3,002	9,513	3225	2257	97925	1645	0,024
C	4	Grinding	T=250	3,001	9,514	3250	2275	2500000	0	0,024
C	5	Grinding	Ref.	3,004	9,511	3200	2237	3647855	0	0,022
C	6	Grinding	Ref. point	3,000	9,512	3250	2277	5069	1645	0,044
C	7	Grinding	Ref.	3,001	9,497	3350	2350	786	1638	0,038
C	8	EDM	3 step	3,124	9,498	1450	939	68519		0,251
C	9	EDM	3 step	3,134	9,503	1475	948	78069		0,241
C	10	Sinter		3,163	9,498					
C	11	Grinding	Ref.	3,004	9,510	3250	2272	4600	1645	0,025
C	12	Grinding	Ref.	3,000	9,515	3300	2313	2447797	1667	0,028
C	13	Grinding	Ref.	3,004	9,515	3250	2270	73193	1652	0,024
C	14	Grinding	Ref. point	3,003	9,515	3250	2272	6722	1645	0,029
C	15	Grinding	T=250	3,004	9,509	3250	2272	2500000	0	0,031
C	16	Grinding	Ref.	3,005	9,513	3700	2584	6971	1602	0,025
C	17	EDM	1 step	3,140	9,498	1400	897	85627		0,388
C	18	EDM	1 step	3,149	9,500	1400	892	79123		0,315
C	19	Sinter		3,187	9,500					
C	20	Sinter		3,149	9,501					

## 6. CEMENTED CARBIDE GRADES

Gegevens voorkeursoorten ( afgeleid van TDB ).

Norm	P1020	P1033	P1026	P1024	P1030	P1022	P1036	P1034
Aanduiding	Co15M	Co15F	Co12M	Co9M	Co9F	Co6F	Co3F	Co3S
Belangrijke Keuzegegevens								
Hardheid ( HV )	1200	1300	1300	1400	1550	1700	2000	2300
Buigsterkte, TRS, ( GPa )	3.0	3.4	2.8	2.7	3.0	2.4	2.4	2.8
Druksterkte ( Gpa )	4.0	4.8	4.6	5.2	5.9	6.7	8.2	9.0
Elasticiteits-modulus ( Gpa )	540	530	580	590	580	640	670	670
Dichtheid	14.0	14.0	14.3	14.6	14.5	14.9	15.2	15.2
Lineaire uitzettings-coëfficiënt ( $10^{-6}/K$ ) tussen 20 en 400 ° C.	6.0	6.2	5,6	5.3	5.5	4.6	4.4	4.4
Warmtegeleidingscoëfficiënt ( W/m.K )	65	65	70	75	75	80	84	84
Soortelijke warmte ( J/kg.K )	220	220	215	210	210	205	200	200
Soortelijke weerstand ( $10^{-8}\Omega.m$ )	17	17	18	19	19	20	21	21
Constante van Poisson	0.23	0.23	0.23	0.23	0.23	0.24	0.24	0.24
Korrelgrootte ( $\mu m$ )	1.3-2.5	0.8-1.3	1.3-2.5	1.3-2.5	0.8-1.3	0.8-1.3	0.8-1.3	0.5-0.8
Gew. % Co	14-16	14-16	11-13	8-10	8-10	5-7	2-4	2-4

## 7. SUPPLIER CODES

Kontaktgroep	Overview of	ESR-1QBG/GR01
Productie	released hardmetal grades	2
Metaalwaren	According to UN-P-standards	2008-04-15

This sheet serves exclusively for use WITHIN THE K.P.M. as information to tool-suppliers and purchasers and must on no condition be handed to others than these.

### 1 Scope

This document specifies the manufacturers, supplier(s) and trade name(s) from which the hardmetal UN-P-grades must be obtained.

The grades below that are marked grey, just have been released partially (1st release), or have not been tested recently, and may only be used by toolmakers after permission of the ordering K.P.M.-customer.

### 2 Suppliers / trade names

Philips standard	Ceratizit Luxemburg	Ceratizit Zwitserland	Ceratizit Oostenrijk	Hoybide	Teco	Hartmetal I AG	Tribo Hartmetall GMBH	Kennametal E.P.G. (NHF)	Kennametal E.P.G. (Widia)	Boehlerit Oostenrijk
	Ceratizit Nederland	Ceratizit Nederland	Ceratizit Nederland	Carbitec	Carbitec	Carbitec	Tribo Hartmetall	Kennametal E.P.G.	Kennametal E.P.G.	Böhler Nederland
UN-P1020	GC30	GC30	H50S	N7	T16D	RG30				
UN-P1022	GC05		H20S		TC4M	RKF	H20 Ti	KF1	THMF	HB10
UN-P1024			H30S	N4	TC8		V20 Ti	K25	GT2H	
UN-P1025	KR 17									
UN-P1026	GC20	GC20	H40S		TC10					
UN-P1030	MG18	MG18	TSM33		TC510	RX10		KMF		
UN-P1033	MG30		MG30		TC515					
UN-P1034	SMG02									
UN-P1036	MG06							O2F		
UN-P1038			CF-H40S							MB20EDM
UN-P1039			CF-H25S							

### 3 Validity

Responsibility for update and distribution of this overview will be taken by K.P.M. This release overview replaces ESR-1QBG/GR01, issued on 2007-06-01.

Kontaktgroep	<b>Overview of</b>	<b>ESR-1QBG/GR01</b>
Productie	<b>released hardmetal grades</b>	2
Metaalwaren	<b>According to UN-P-standards</b>	2008-04-15

UN P1038 and UN P 1039 are coming standards for corrosion resistance hardmetal. These types of hardmetals have comparable mechanical properties but are significantly less affected by (worse conditioned) wire erosion processes.

Hoybide and Teco have shown some serious problems with their quality level related to hardmetal supplies. Although this has not been fully proven for all grades, the KPM cannot recommend these suppliers any longer as a producer of a consistent quality of hardmetals. As such, the KPM marked Hoybide and Teco grey in the table shown in paragraph 2.

## 8. P1030 STANDARD

OG CSD: 2020	STANDARD	
Standards & Environment	<b>HARDMETAL</b> <b>Co9-F</b>	<b>UN-P 1030</b> page 1/3 EN 2002-08-31
<b>CSD</b>		

Supersedes UN-P 1030 dated 2001-01-31

Keywords: metals; hardmetals; carbides; cemented carbides;  
sintered products; metal forming

### 1 Scope

This standard specifies the requirements on hardmetal Co9-F in the sintered and hot isostatic pressed or "sinter-hipped" condition.

This standard conforms to requirements of Philips specifications, as international or national standards do not exist.

### 2 Composition

Tungsten carbide with:

Co Cobalt : 8 % - 10 % by weight.

Other carbide forming elements  
(V, Cr, Ta, Nb), together : max. 1 %

All other elements together : max. 0,3 % of which  
Fe Iron : max. 0,15 % and  
Each other element : max. 0,1 %

### 3 Sintered parts

#### 3.1 Properties

##### 3.1.1 Structure (derived from ISO 4499)

The structure shall correspond with  $\alpha$ -fine and shall preferably be free from  $\gamma$ -phase. If the structure contains  $\gamma$ -phase, this phase shall be regularly distributed  $\gamma$ -fine.

The structure shall be homogeneous.

At least 90 % of the carbide volume shall consist of carbides with a grain size between 0,8  $\mu\text{m}$  and 1,3  $\mu\text{m}$  (F = fine grain).

Grain size

4,0  $\mu\text{m}$  - 6,5  $\mu\text{m}$  : max. 40/mm<sup>2</sup>  
> 13,0  $\mu\text{m}$  : not allowed

Neither carbide conglomerations nor cobalt-lakes are allowed.

The  $\eta$ -phase shall be absent.

##### 3.1.2 Mechanical properties

Property	Value	Unit	Test standard
Vickers hardness	1500 - 1650	HV30	ISO 3878
Rockwell hardness <sup>1)</sup>	91,2 - 92,2	HRA	ISO 3738
Palmqvist toughness	min. 700	kN/m	UN-L 1188
Transverse rupture strength <sup>1)</sup>	3,0	GPa	ISO 3327

<sup>1)</sup> For information only.

##### 3.1.3 Physical properties

Property	Value	Unit	Test standard
Mass density	14,3 - 14,7	g/cm <sup>3</sup>	ISO 3369
Porosity	max. A02 B00	-	ISO 4505
Number of pores per cm <sup>2</sup> with a size between 10 $\mu\text{m}$ - 25 $\mu\text{m}$	max. 10	-	ISO 4505
Uncombined carbon	better than C02	-	ISO 4505

#### 3.2 Quality and finish

The products shall be supplied to a constant quality. With the exception of the machining allowance, the products shall be uniform in composition, structure and properties.

### 3.3 Machining allowances and their tolerances

#### 3.3.1 Normal sizes up to 20 mm

Class	Machining allowance [mm]		Tolerance [mm]
	Outside dimensions	Inside dimensions	
X	0/+0,6	0/-0,6	0/+0,4 0/-0,4
Y	0/+0,6	0/-0,6	0/+0,4 0/-0,4
Z	0	0	0/+0,2 0/-0,2

#### 3.3.2 Nominal sizes over 20 mm

Class	Machining allowance [mm]		Tolerance % of the nominal size
	Outside dimensions	Inside dimensions	
X	0/+0,6	0/-0,6	0/+1 0/-1
Z	0	0	0/+1 0/-1

### 3.4 Delivery

The products shall be packed in such a way that they are protected against damage and contamination in transit. Each part shall be marked with grade (P 1030) and manufacturer. Requirements concerning the method of packing shall be agreed upon between supplier and consumer.

### 3.5 Order data

In the order shall be stated:

drawing number :  
 designation and standard : Co9-F UN-P 1030  
 number of pieces :  
 allowances and tolerances : class X, Y or Z (par. 3.3)  
 packing : to be agreed upon  
 certificate : to be agreed upon

### Explanation

With regard to edition UN-P 1030 dated 2001-01-31 modifications are:

- Fracture toughness has been changed into Palmqvist toughness as a parameter for resistance to crack-growth. This value has been adapted and will be a functional test requirement;
- Reference to UN-L 1188 "Measuring the Palmqvist toughness of hardmetals" has been adapted.

## 9. CERATIZIT TEST REPORT

### Werkzeugnis 2.2 – Test Report 2.2

nach / according to EN 10204:2005



<b>Abteilung / Department</b>		<b>Bescheinigungs-Nr. / Certificate No.</b>		<b>Datum / Date</b>	
WT / B. Marklein		3500462		04.11.2010	
<b>Kunde / Customer</b>			<b>Kundenbestell-Nr. / Customer Order No</b>		
B&S Technology					
<b>Produkt / Product</b>		<b>Ident-Nr. / Identity No</b>			
Carbide Blanks for blanking and lamination tools 100x100x3 mm		6102536			
<b>Auftrags Nr. / Job No</b>	<b>Sorte / Grade</b>	<b>Charge / Lot</b>	<b>Liefermenge / Quantity</b>		
6721311	MG18	6096	3		

#### Chemische Zusammensetzung / Composition

<b>WC Korngröße / WC Grainsize</b>	Submicron
<b>WC</b>	Rest / Balance
<b>Co</b>	10 %
<b>Cr<sub>2</sub>N</b>	0,57 %
<b>others</b>	0,2 %

#### Physikalische Eigenschaften / Metallurgical Data

			<b>Soll / Expected Values</b>	<b>Ist / Measured Data</b>
<b>Koerzitivfeldstärke / Coercivity</b>	[da A/m]	ISO 3326	2150 ± 240	2141
<b>Härte / Hardness</b>	[HV30]	ISO 3878	1660 ± 60	1625
<b>Dichte / Density</b>	[g/cm <sup>3</sup> ]	ISO 3369	14,45 ± 0,12	14,38

#### Porosität / Porosity (ISO 4505)

	<b>Soll / Expected Values</b>	<b>Ist / Measured Data</b>
<b>A</b>	02	<02
<b>B</b>	00	00
<b>C</b>	00	00

#### Bemerkungen / Remarks

Lieferschein- Nr. / Delivery note: 87366810

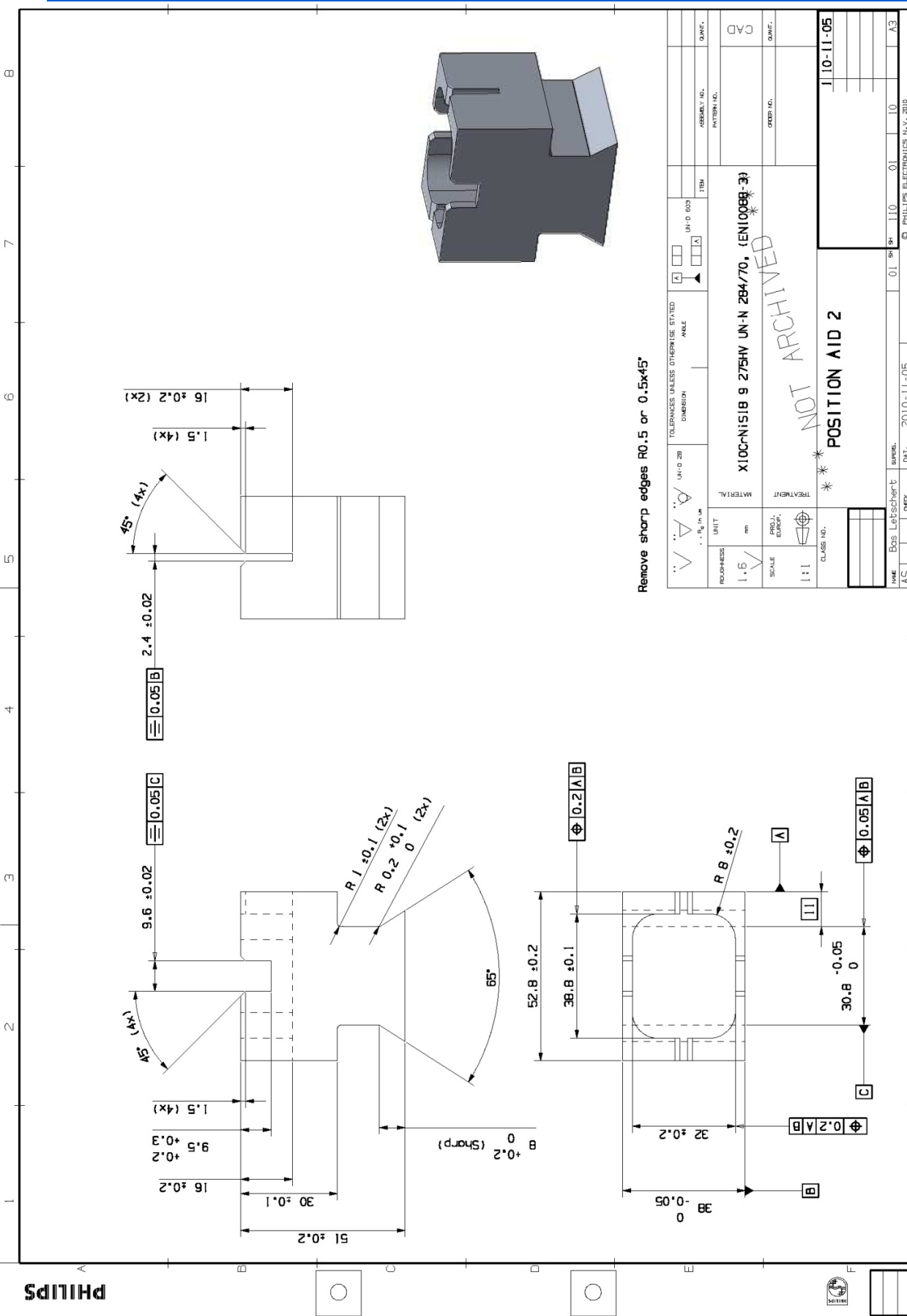
Es wird bestätigt, dass die Lieferung den Vereinbarungen bei der Bestellung entspricht.  
We hereby certify that the delivered product above complies with the terms of order.

**QM-System:**  
**Zertifiziert nach ISO 9001:2008**  
**Certified according to ISO 9001:2008**

Bernd Sprenger  
für / for CERATIZIT

**CERATIZIT Deutschland GmbH**  
Robert-Bosch-Straße 23  
D-72186 Empfingen  
Tel. +49 7485 99802 0

10. POSITION AID



Remove sharp edges R0.5 or 0.5x45°

PROFESSOR	UNIT	MATERIAL	TREATMENT	CLASS NO.
1:6	mm	X100C-NiSi18 9 275HV UN-N 284/70, (EN10088-3)		
SCALE	PROJ. CORP.			
1:1				
** NOT ARCHIVED **				
POSITION AID 2				
J 10-11-05				
NAME	DESIGN	DATE	REV	QTY
Bas Leitschert	2010-11-05	01	01	10
PHILIPS ELECTRONICS N.V. 2010				